JOURNAL OF PETROLOGY

Journal of Petrology, 2018, Vol. 59, No. 12, 2493–2518
doi: 10.1093/petrology/egy025
Advance Access Publication Date: 1 March 2018
Original Article

OXFORD

Petrography of Snap Lake Kimberlite Dyke (Northwest Territories, Canada) and its Interaction with Country Rock Granitoids

Alexandrina Fulop[1]*, Maya Kopylova[2], Stephan Kurszlaukis[1], Luke Hilchie[2,†], Pamela Ellemers[1] and Charlene Squibb[3]

[1]De Beers Canada, Mining Technical, 300-1601 Airport Road NE Calgary T2E 6Z8, Canada; [2]Department of Earth, Ocean and Atmospheric Sciences, University of British Columbia, 2207 Main Mall, Vancouver V6T 1Z4, Canada; [3]De Beers Canada, Gahcho Kue Mine, 300-5120 49th Street, Yellowknife X1A 1P8, Canada

*Corresponding author. Telephone: +1 403 930 0991 ext. 2705. E-mail: alexandrina.fulop@debeersgroup.com
[†]Present address: Department of Earth Sciences, Dalhousie University, 1459 Oxford Street, PO BOX 15000, Halifax, Nova Scotia, B3H 4R2, Canada

Received November 1, 2015; Accepted February 21, 2018

ABSTRACT

Carbonate-rich intrusions in contact with felsic rocks theoretically should show the effects of interaction between the two rock types, due to their contrasting compositions. In reality, though, such interaction is rarely reported at kimberlite contacts. We present the first documented case of lithological and mineralogical zonation at the margin of a kimberlite, the Snap Lake dyke, in contact with the wall-rock granitoid. Our detailed petrographic, mineralogical and geochemical study shows that the fresh hypabyssal kimberlite consists of olivine macrocrysts and microcrysts, and phlogopite macrocrysts set in a groundmass of serpentinized monticellite, phlogopite, spinel, perovskite and apatite, with interstitial lizardite and calcite. This typical Group I kimberlite mineralogy does not match the bulk-rock composition, which resembles a Group II micaceous kimberlite. The mismatch between the chemical and mineralogical properties is ascribed to contamination by granitoid xenoliths and metasomatic reactions with the felsic country rocks, the Snap Lake kimberlite has extremely low bulk-Ca compared to other documented Group I kimberlites. Reaction with deuteric H_2O and CO_2 has led to Ca removal, serpentinization of olivine, replacement of calcite by dolomite, alteration of perovskite and decomposition of apatite. Adjacent to the contact with the host granitoid and in haloes around granitoid clasts, poikilitic phlogopite and lizardite are replaced by subsolidus phlogopite and a multiphase phyllosilicate composed of phlogopite+ lizardite+ chlorite+ talc. A modified isocon analysis accounts for felsic xenolith assimilation and isolates metasomatic changes. Enrichment of altered kimberlites in Si owes solely to xenolith incorporation. The metasomatic ingress of granitoid-derived Al for a limited distance inside the dyke was counteracted by a flux of Mg and Fe to the granitoid. Metasomatic changes in K and Ca tend to be positive in all lithologies of kimberlite and in the granitoids implying distal transport. The combination of xenolith digestion with metasomatic element transport is expected in hybrid zones where kimberlite magmas interact with felsic wall-rocks.

Key words: xenolith contamination; metasomatism; kimberlite-granitoid contact; phlogopite; recrystallization; Snap Lake kimberlite; isocon analysis

INTRODUCTION

When carbonate-rich and felsic rocks are juxtaposed at high subsolidus temperature, their contrasting elemental chemical potentials trigger metasomatism. This commonly produces skarns (when the intrusion is felsic) or fenites (when the magma is carbonatitic). Fenitization is widely documented at the outer borders of syenites, carbonatites and other alkaline intrusions,

but rarely replaces carbonatites. Although carbonate-rich intrusions are highly reactive (Meinert *et al.*, 2005), only one occurrence of contact metasomatism has been reported within a carbonatite, a wollastonite zone in the Alnö carbonatite (Skelton *et al.*, 2007). Moreover, similar alteration and contact kimberlite breccias with alkali amphiboles and pyroxenes (Smith *et al.*, 2004) are rarely documented at the kimberlite contacts (Le Bas, 2008), being restricted to only few African kimberlite pipes (Ferguson *et al.*, 1973; Smith *et al.*, 2004). Although some kimberlites are well exposed due to mining, metasomatic effects in them are difficult to isolate because of the common presence of marginal country-rock breccias (Clement, 1982) and assimilated country-rock xenoliths.

Kimberlites in contact with felsic gneisses or granitoids should theoretically develop metasomatic alteration, replacing both the felsic wall-rocks and the silica-undersaturated magmatic rocks. The goal of this study is to report an example of rarely documented metasomatism at the contact of a kimberlite with silicic wall-rocks and to isolate the metasomatic effects from those of physical contamination. We based the study on the Snap Lake dyke, which is exceptionally well sampled and geologically well documented, due to years of exploration and mining. The Snap Lake kimberlite dyke, dated at 523 +/- 6·9 Ma (Rb-Sr isochron; Heaman *et al.*, 2004), is located in the south–central Slave Craton of northern Canada and intrudes granitoids and mafic amphibolite-bearing metavolcanic rocks (further called 'metavolcanics') of greenschist facies that belong to the >2·8 Ga (Stubley, 2000, unpublished data) Camsell Lake greenstone belt. We describe the petrography, mineralogy and geochemistry of the kimberlite, classify it into several alteration zones and thoroughly document the spatial relationships between the alteration zones and the country-rocks. This study is based on hundreds of samples, a variety of datasets and systematic profiles through the contacts, and, as such, is more comprehensive than previous publications on the Snap Lake kimberlite (Field *et al.*, 2009; Kopylova *et al.*, 2010; Gernon *et al.*, 2012). We show that xenolith contamination and metasomatic interaction along the contacts between kimberlite and felsic country rocks recrystallizes the kimberlite and alters the granitoid.

SAMPLE COLLECTION AND ANALYTICAL TECHNIQUES

The geology of the Snap Lake dyke was investigated in more than 100 drill cores (approximately 1000 m), and

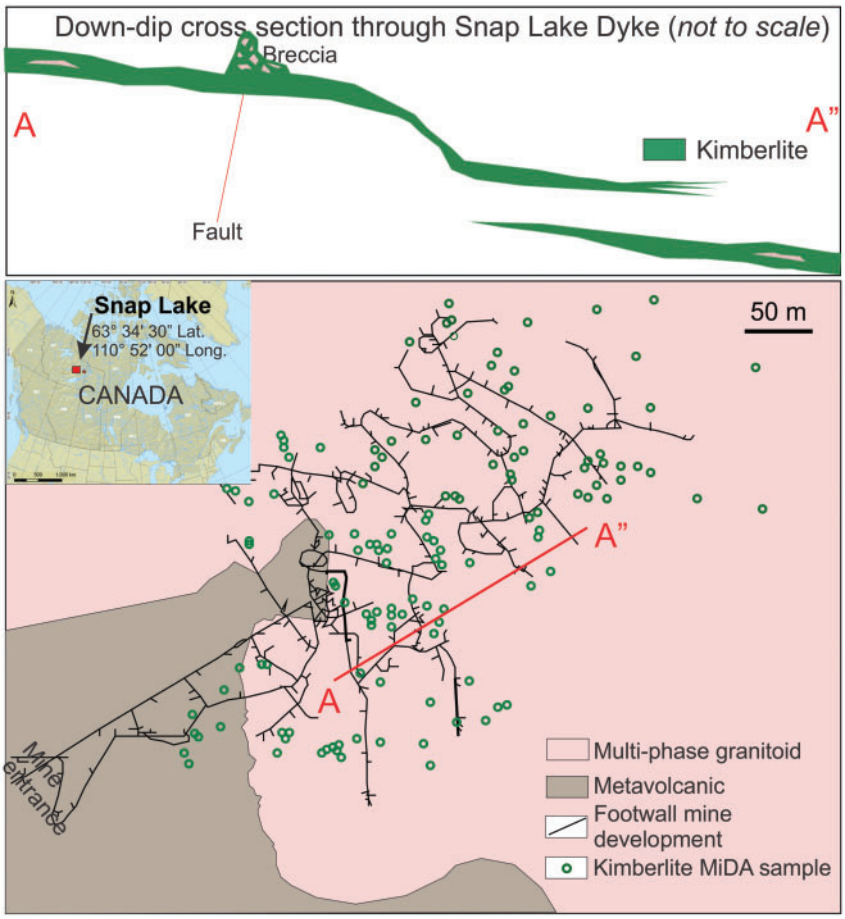

Fig. 1. Schematic cross-section of the Snap Lake dyke along line A–A' and a plan view of microdiamond sampling locations and mine tunnels for the studied specimens.

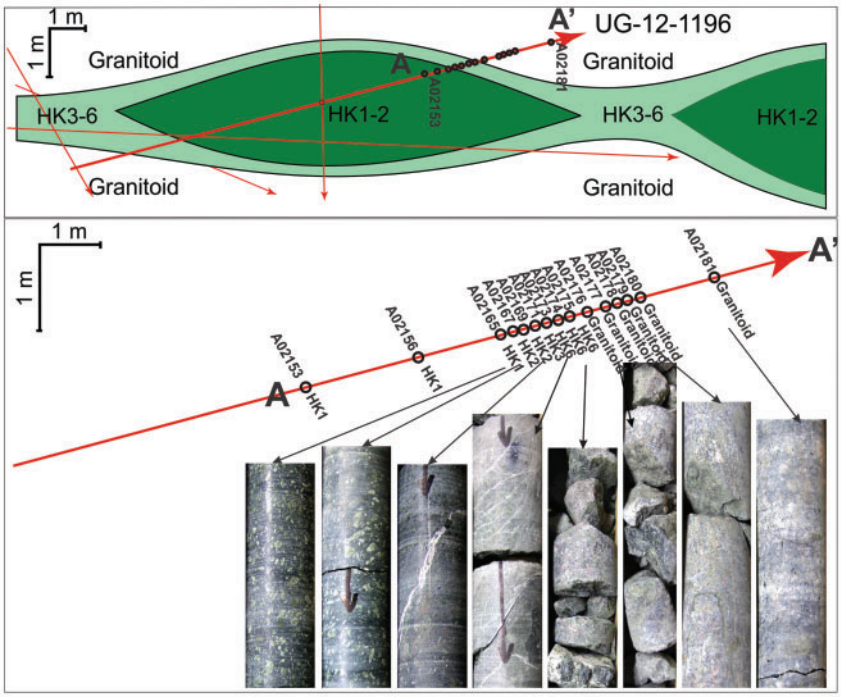

Fig. 2. Sampling across the kimberlite-granitoid contact. The shape of the dyke and the rock types are constrained based on drill holes. Locations of samples in drill core UG-12-1196 are marked by open circles. The enlarged area shows the locations of samples along the A–A′ profile and photographs of the analyzed core which has a standard width of 4 cm.

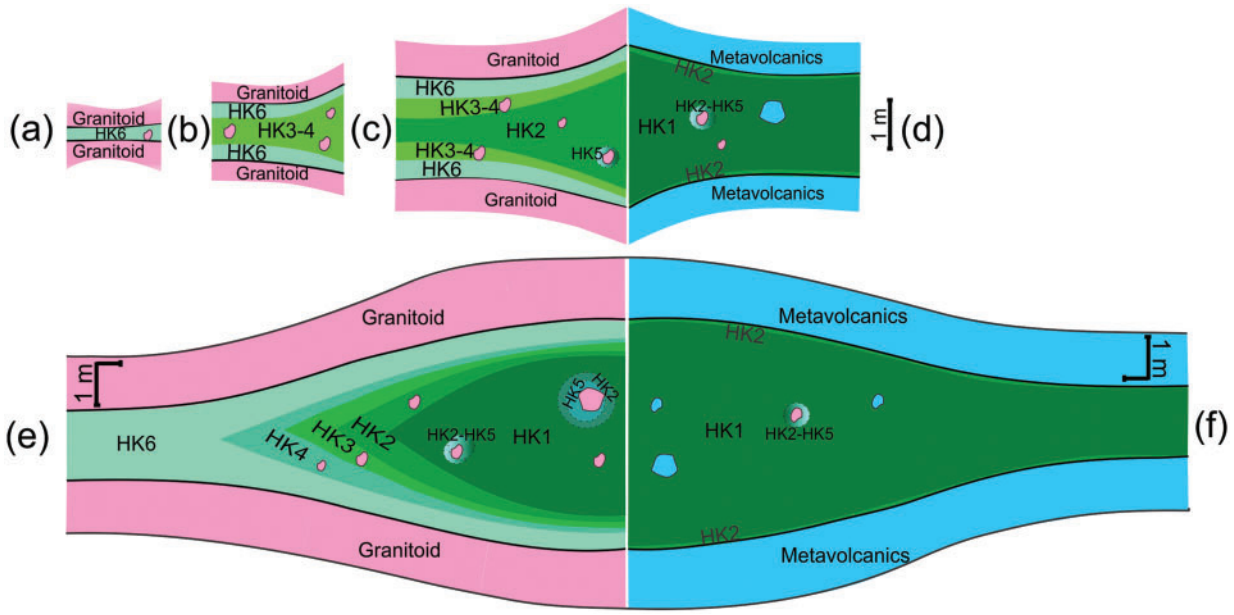

Fig. 3. Cross-sections through the dyke at locations with varied dyke thicknesses, from 0·1 to 3 m (a–f). Schematic generalized cross-section through the dyke hosted by granitoid (a,b,c,e) and metavolcanics (d,f). The granitoid in a ~1 m-wide area around the dyke is altered, brecciated and cross-cut by kimberlite veinlets. The distribution of the rock types was documented in 20 drill cores cross-cutting the dyke at 90° and subsequently confirmed in drill cores that intersect the dyke at a shallow angle. In addition, over 30 underground face maps allowed accurate measurements of the dyke thickness. Dyke intersections with metavolcanics were investigated in five drill cores and three underground face maps.

30 mapped underground faces (approximately 300 m^2). The sampling locations (Figs 1–3) were chosen to ensure a good lateral coverage of the dyke at different dyke thicknesses, in all alteration zones, and all country-rock lithologies. Samples were also collected from the country-rocks and along one profile through the kimberlite-granitoid interface (Fig. 2). The logged drill core and mapped faces were subsequently examined

petrographically (400 thin sections) and further analyzed for whole-rock major and trace elements (370 samples), mineral compositions (60 thin sections), powder and single-crystal X-ray diffractometry (20 samples) and microdiamond content.

An electron-microprobe investigation of mineral composition was based on 60 thin sections and resulted in collection of 200 analyses of phlogopite and other sheet silicates (Supplementary Data Table S1 (EST1); 100 analyses of groundmass spinel and 50 analyses of groundmass apatite (Supplementary Data Table S2 (EST2)). The analyses were carried out at the University of Toronto (Canada) on a Cameca SX-50/51 (DCI 1300 DLL)) equipped with three tunable wavelength dispersive spectrometers. The analytical conditions for the sheet silicates were 15 keV accelerating voltage, 15 nA beam current and a 5 μm beam size. The on-peak and off-peak counting times were 20 seconds for all elements except Mn (40 secs). Unknown and standard intensities were corrected for deadtime. Standard intensities were corrected for standard drift over time. Oxygen was calculated by cation stoichiometry and included in the matrix correction. Oxygen equivalent for halogens (F/Cl/Br/I) was subtracted in the matrix correction. The matrix correction method was ZAF or Phi-Rho-Z algorithm (See & Armstrong, 1988). For spinel and apatite analyses, an accelerating voltage of 20 keV, a beam current 20 nA and a beam diameter of 1 micron were used. The counting time on-peak and off-peak for all elements was 10 seconds, the off peak correction method was linear for all elements.

Carbonates, olivine and perovskite (Supplementary Data Table S2 (EST2)) were analyzed at the Earth, Ocean and Atmospheric Sciences Department, University of British Columbia (UBC), using a fully automated CAMECA SX50 microprobe. Carbonates were analyzed using an accelerating voltage of 15 kV, beam current of 10 nA and a beam diameter of 5 μm, a uniform peak counting time of 20 seconds and background counting time of 10 seconds. Alkali elements were analyzed first to minimize loss and possible underestimation. Perovskite and olivine were analyzed using an acceleration voltage of 15 kV, beam current of 20 nA, beam diameter 1–3 μm, peak counting time of 20 seconds and background counting time of 10 seconds.

Three hundred and seventy samples of kimberlite and country-rocks were analyzed for major and trace elements (Supplementary Data Table S3 (EST3)) at Acme Labs (Vancouver, Canada) using Inductively Coupled Plasma Emission Spectrometers (ICP-ES) Spectro Ciros Vision and Nexion 300. Prepared samples were mixed with $LiBO_2/Li_2B_4O_7$ flux, fused in a furnace and then dissolved in nitric acid and analyzed. Loss on ignition (LOI) was determined by igniting a sample split then measuring the weight loss. Total carbon was determined by the Leco method, and total Fe was reported as Fe_2O_3. All major elements had minimum detection limits (MDL) of 0·01 wt %, except K_2O and Fe_2O_3 (0·04 wt %). Barium was also analysed by ICP-ES with an MDL of 5 ppm. The analysis of trace elements was carried out using an Inductively Coupled Plasma Mass Spectrometer Elan 9000, with the following MDLs: 20 ppm (Ni), 8 ppm (V), 1 ppm (Zn, Be, Sc), 0·5 ppm (Ga, Sr, W), 0·3 ppm (Nd), 0·2 ppm (Co, Th), 0·1 ppm (Cu, Pb, Ce, Cs, Hf, la, Nb, Rb, Ta, U, Y, Zr), 0·05 ppm (Dy), 0·02 ppm (Eu, Ho, Pr) and 0·01 ppm (Lu, Tb, Tm).

Powder X-ray diffraction analysis was performed on 20 highly altered bulk samples rich in serpentine and phlogopite. The analysis was carried out at Acme Labs (Vancouver) using a Siemens D500 Diffractometer and MDI Data Scan and JADE 8 Software. A predetermined amount of sample was hand ground and mixed with acetone to produce a thin slurry. The mixture was applied onto a glass slide, analyzed and reported as semi-quantitative levels of minerals, from 'trace' to 'abundant'. Powder X-ray diffraction measurements were also made for grains drilled out from polished thin sections. These analyses were made at the Structural Chemistry Facility, Department of Chemistry, UBC, using a Bruker APEX DUO diffractometer with graphite monochromated CuK $\gamma-$radiation. Data were collected at room temperature as a series of three still frames at different 2 theta values. The sample-to-detector distance was set to 180 mm and the sample rotated 360° about the axis during the 300 s exposure time for each frame. The three frames were merged together to give a total 2 theta range of ~5° to 60°, and integrated to give a powder diffraction pattern. The data were analyzed using the Bruker EVA program.

Microdiamond caustic fusion analysis was performed at the Saskatchewan Research Council (SRC) in Saskatoon (Canada). One hundred seventy samples of kimberlite (each sample weighing eight kg) were fused in a kiln containing caustic soda; the hot residues were then poured through sieves and chemically treated to reduce them to a manageable size. Diamonds were recovered from the final residues, sieved and weighed. The weighing of stones was performed using Ultra Micro Analytical balances which have scheduled external ISO/IEC 17025: 2005 calibrations and daily calibration checks for quality assurance, a method which is accredited by the Standards Council of Canada, CAN-P-4E - ISO/IEC 17025: 2005. The quality of the method was monitored by assessing the recovery of the synthetic diamonds added to the sample during the caustic fusion and chemical treatment processes.

KIMBERLITE GEOLOGY

The Snap Lake dyke dips at ~15° to the northeast (Fig. 1) and has an average thickness of 2·8 m, as constrained by underground drilling and mapping. It extends over a known distance of 3·5 km in a north–south direction and 2·4 km in an east–west direction. The contact between the host metavolcanics and the underlying granitoids is crossed by the dyke at a depth of ~140 m, 900 m to the northeast of the dyke's surface outcrops and subcrops. The dyke thickness decreases

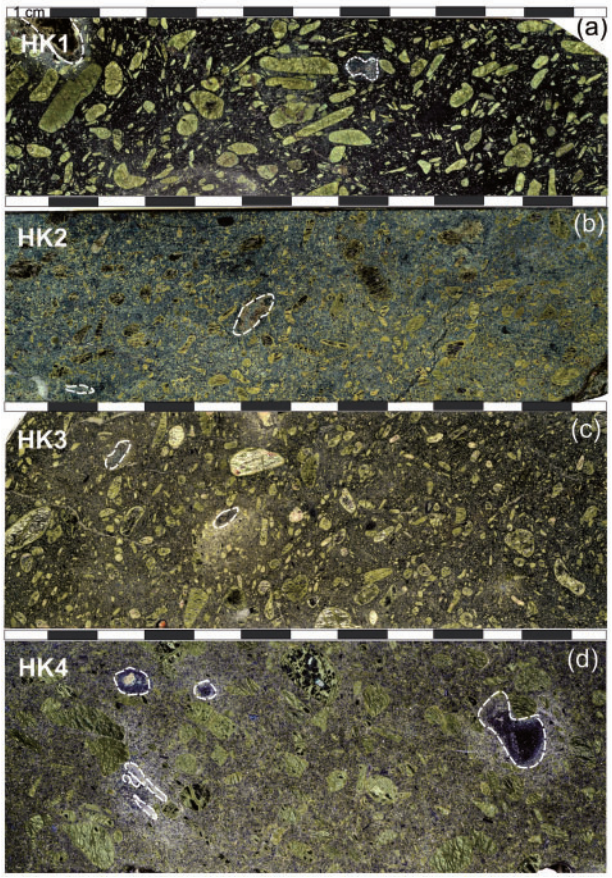

Fig. 4. Photographs of Snap Lake kimberlite slabs. (a) Coarse-grained serpentinized macrocrystic kimberlite HK1. (b) Medium grained serpentinized macrocrystic kimberlite HK2. (c) Medium grained serpentinized macrocrystic kimberlite HK3. (d) Medium grained serpentinized macrocrystic kimberlite HK4. White dashed contours outline assimilated granitoid xenoliths.

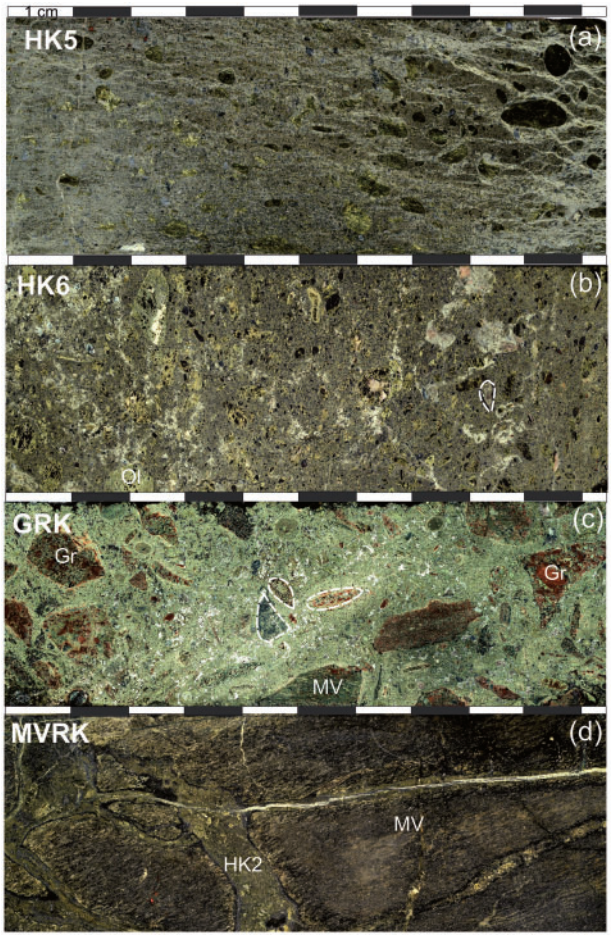

Fig. 5. Photographs of Snap Lake kimberlite and breccia slabs. (a) Medium grained serpentinized altered kimberlite HK5 cross-cut by thin braided veins. (b) HK6 with medium to fine grained altered olivine and the groundmass with white patches of carbonate and talc alteration. (c) GRK with abundant, variously assimilated granitoid xenoliths. Dark colour xenoliths are minimally altered, whilst an angular, strongly assimilated elongate xenolith (white dashed outline) does not have sharp boundaries and is surrounded by a light reaction halo. Light coloured mineral in the groundmass is carbonate. (d) Metavolcanics-dominated kimberlite (MVRK) with large angular clasts of mafic amphibolite facies metavolcanics.

outward from a central axis trending roughly NE–SW. The dyke is continuous as a whole, but segmented in the south–central area by at least one major split that bifurcates towards the SE (Fig. 1). Also, at a small scale, the dyke splits into multiple thinner kimberlite veinlets, scattered over tens of meters, without continuity in between.

The Snap Lake dyke comprises volumetrically prevalent hypabyssal xenolith-poor kimberlite (HK) and two types of xenolith-rich kimberlites: Granitoid-rich Kimberlite (GRK, with up to 50% granitoid xenoliths) and MetaVolcanic-rich Kimberlite (MVRK, with up to 85% metavolcanic xenoliths).

Examination of dyke cross sections and macrospecimens reveals contrasts between competent magnetic HK away from the dyke contacts and less competent, less magnetic HK in contact with the host granitoid. The former has a dark green groundmass and distinctive yellowish gray pseudomorphs after macrocrystal olivine (Figs 2 and 4a), whereas the latter shows a smaller colour contrast between the grey pseudomorphed olivine and the greenish grey groundmass (Figs 2 and 5b).

Previous classification schemes for the Snap Lake kimberlite referred to these two types of HK as olivine-rich and olivine-poor, and interpreted them as crystallizing from distinct magma batches (Field *et al.*, 2009; Gernon *et al.*, 2012). However, our examination of the HK types revealed microscopic, gradual transitions between alteration zones of a single HK rock type. Fresh hypabyssal kimberlite (HK1) in the center of the dyke (Fig. 4a) grades into altered kimberlite (HK6) at the contact with the host granitoid (Fig. 5b) through consecutive zones (HK2, 3, 4) parallel to the dyke walls (Figs 3e, 4b–d). The textures and mineralogy of these zones are described in the following section. The thickness of the zones is largely controlled by the thickness of the dyke. Zones HK3, 4, and 6 comprise the entire dyke where it is thinner than 1·5–2 m (Fig. 3a, b). As the thickness of the dyke increases, HK1 and 2 occur in the center of the

dyke (Fig. 3c, e). The same progression of alteration zones develops in centimeter-wide zones around granitoid xenoliths. HK5 is constrained to such a context, developed in the center of the dyke (Figs 3c–f, 5a). It is important to note that progressive changes in the kimberlite mineralogy and texture towards the dyke margins are not observed where the dyke intrudes metavolcanics, i.e. in the shallower, NW part of the dyke. Here the dyke shows exclusively HK1–2 zones, irrespective of the dyke thickness (Fig. 3d, f).

Xenolith-rich kimberlite (GRK and MVRK) occurs in the vicinity of faults and contains a xenolith population that corresponds to the local country-rock. GRK typically contains 40–60 vol. % granitoid clasts (3–5 cm) set in a coherent hypabyssal kimberlite groundmass similar in texture to HK6 (Fig. 5c); MVRK comprises relatively fresh kimberlite (HK1–2) containing up to 50–85% metavolcanic xenoliths composed of amphiboles and feldspars (Fig. 5d). MVKR is rarely encountered because only ~10% of the mapped dyke intrudes metavolcanics.

PETROGRAPHY

Fresh hypabyssal kimberlite HK1

The kimberlite is composed of serpentinized olivine macrocrysts and microcrysts, phlogopite macrocrysts, groundmass minerals, and mesostasis (Table 1). Fresh olivine is very rare (Fig. 6b). Phlogopite macrocrysts form long euhedral laths, or short tabular, euhedral to anhedral crystals with irregular margins and a fine-grained magnetite-rich reaction rim (Fig. 6e). The groundmass contains monticellite pseudomorphs, phlogopite, spinel, perovskite and apatite crystals set in a mesostasis of cryptocrystalline serpentine, chlorite, and calcite (Table 1; Fig. 6a–c; Supplementary Data Fig. S2). Monticellite, the dominant groundmass mineral, is entirely serpentinized, but preserves the typical subhedral to anhedral isometric shape (Fig. 6a–d; Supplementary Data Fig. S2). Spinel forms composite 'atoll' crystals with discrete cores and mantles, or single euhedral or subhedral crystals. Perovskite occurs as euhedral zoned crystals. Apatite typically forms radial clusters of individual long prismatic euhedral crystals, poikilitically enclosing spinel and monticellite pseudomorphs. The interstitial mesostasis comprises cryptocrystalline lizardite and chlorite, with spinel inclusions and rare poikilitic calcite grains (Fig. 6b). Phlogopite in the groundmass forms long euhedral poikilitic laths with inclusions of groundmass serpentinized monticellite and spinel (Fig. 6a–c; Supplementary Data Fig. S2), and develops only in the proximity of granitoid xenoliths (Fig. 6d, e; Supplementary Data Fig. S2).

Thin, post–emplacement veins cutting through olivine macrocrysts and the groundmass of serpentine and carbonate develop subparallel to the contact 30–50 cm away (Fig. 2).

Highly altered kimberlite HK6

The kimberlite in contact with granitoid is an equigranular rock made of tabular grains of a cryptocrystalline, multiphase phyllosilicate, optically resembling phlogopite (Fig. 7b–d). The exact nature of this phase is discussed in section "Identification of phyllosilicates". The phyllosilicate grains are occasionally larger if they are pseudomorphing olivine (Fig. 7c, d; Supplementary Data Fig. S4) or monticellite (Fig. 7c, d; Supplementary Data Fig. S5). The rock shows abundant veins of multiphase phyllosilicate that forms buckling wavy crystals with veering cleavage (Fig. 7e, f) and the higher birefringence of talc. Post-emplacement braided carbonate veins develop at the contact (Fig. 2).

Mineralogical and textural zoning between HK1 and HK6

The following gradual changes occur between fresh HK1 and highly altered HK6 in zones HK2–HK5 (Table 1):

- Replacement of olivine and monticellite by serpentine, followed by a progressive replacement of serpentine by multiphase phyllosilicate (phlogopite + lizardite + chlorite + talc), chlorite, carbonate and smectite (Figs 6c–f, 8a–f; Supplementary Data Figs S2–S5);
- Expansion of serpentine replacing olivine and monticellite beyond the original crystal shapes of these minerals (Fig. 8e, f; Supplementary Data Figs S2–S3);
- A decrease in the modes of atoll spinel, apatite and perovskite and their replacement by various phyllosilicates;
- Replacement of radial clusters of apatite with long prismatic apatite grains, and perovskite with rutile and ilmenite;
- Development of veins filled with phlogopite, serpentine, talc and carbonate (Supplementary Data Fig. S6).

More complex changes are observed for phlogopite and other phyllosilicates. The kimberlite groundmass in HK2 appears enriched (compared to HK1) in partially altered, long, poikilitic phlogopite with inclusions of serpentinized monticellite and spinel, which typically occurs in subparallel, rather poorly defined veins or with a random cross-cutting orientation (Fig. 6c, e, f; Supplementary Data Fig. S2). From HK2 to HK3, the phlogopite shape changes from elongate to short tabular, sometimes with poikilitic rims (Fig. 8a, b; Supplementary Data Figs S2–S3). In the HK3 groundmass, phlogopite has short, prismatic, euhedral shapes and may be zoned, with rare dark brown to light yellow cores and colourless rims (Fig. 8a–d; Supplementary Data Fig. S3). This phlogopite is commonly non-poikilitic and tabular (Fig. 8c; Supplementary Data Fig. S3). From HK3 to HK4, phlogopite increases in abundance. The transition to HK6 is indicated by the partial or complete replacement of phlogopite with a cryptocrystalline mix of phyllosilicates (phlogopite + lizardite + chlorite + talc) with swerving cleavage and undulose extinction (Fig. 8e, f; Supplementary Data Fig. S3).

Table 1: Distinctive textural and mineralogical features of the Snap Lake hypabyssal kimberlite

Rock type	HK1	HK2	HK3	HK4	HK5	HK6
Macrocrystal Phl (1–3 mm)	1–2%, euhedral elongate, with rim of fine-grained opaques, rarely overgrown by poikilitic rims	1%, euhedral elongate, with rim of fine-grained opaques, overgrown by serpentine or serpentinized	2%, euhedral, less elongate, never with fine-grained opaque rim or inclusions	<1%, euhedral, less elongate, replaced by serpentine and chlorite, never with fine grained opaque rim or inclusions	Replaced by multiphase phyllosilicate and locally by smectite	Replaced by multiphase phyllosilicate and locally by smectite
Non-poikilitic, short tabular microcrystal Phl	rare, 0·3 mm	up to 5%, 0·3 mm	20–25%, 0·3–0·5 mm	25–50%, 0·3–0·5 mm, partly replaced by serpentine and chlorite	Subordinate to multiphase phyllosilicate	Subordinate to multiphase phyllosilicate
Poikilitic, long prismatic microcrystal Phl	0–3%, 0·1–0·3 mm, may overgrow rare macrocrysts	10– 50%, 0·3–0·7 mm	May overgrow tabular non-poikilitic macro- and microcrystal Phl	May extensively overgrow non-poikilitic tabular macro- and microcrystal Phl	Rare relicts	
Macrocrystal and microcrystal olivine 0·5–1·5 cm, rarely up to 2 cm	25–35%, very rarely (in two samples from 400) fresh, mostly serpentinized	20–25% Serpentinized, rarely replaced by dolomite	20–25% Serpentinized, rarely replaced by dolomite	Serpentine pseudomorphs are further replaced by multiphase phyllosilicate	Replaced by multiphase phyllosilicate and locally by smectite	Replaced by multiphase phyllosilicate and locally by smectite
Microcrystal monticellite replaced by lizardite	60–40%	40%	20%	Not possible to determine as serpentine pseudomorphs expand into the groundmass and distort the original crystal shape	Replaced by multiphase phyllosilicate and locally by smectite	Replaced by multiphase phyllosilicate and locally by smectite
Carbonate	0–10%, calcite and dolomite, 0·2 mm poikilitic grains enclosing spinel	10%, dolomite only	5%, dolomite only, 0·1 mm grains	5%, dolomite only	Mostly in veins	Mostly in veins
Perovskite	1–2%, magmatically zoned, non-ideal stoichiometry	Replaced by rutile and ilmenite	Replaced by rutile and ilmenite	Replaced by rutile and ilmenite		
Spinel, 5%	Often with atoll rims	Often with atoll rims	Rare atoll spinel	Rare atoll spinel		
Apatite	2%, radial clusters	1%, radial clusters	1%, discreet prismatic crystals	1%, discreet prismatic crystals		10% radial clusters in carbonate
Multiphase phyllosilicate (lizardite+chlorite +talc+phlogopite)		Rare as Phl replacement	Replaces serpentine and Phl	Replaces serpentine and Phl	80–100%, replaces all minerals, appears as bent phlogopite crystals	80–100%, replaces all minerals, appears as bent phlogopite crystals
Smectite	Rare	Rare	Rare	Rare	Abundant, localized along or adjacent to faults	Abundant, localized along or adjacent to faults
Granite xenoliths >1 cm Granite microxenoliths (0·5–10 mm)	0·5–5% 0·5–1%, mostly assimilated	1–15% 1–2%, assimilated, fresh to altered	5–10% 5%, mostly assimilated	10% 5–10% assimilated, fresh to altered	10–15% 2–5% assimilated, fresh to altered	10–15% >10%, assimilated, fresh to altered

Phl here and further stands for phlogopite.

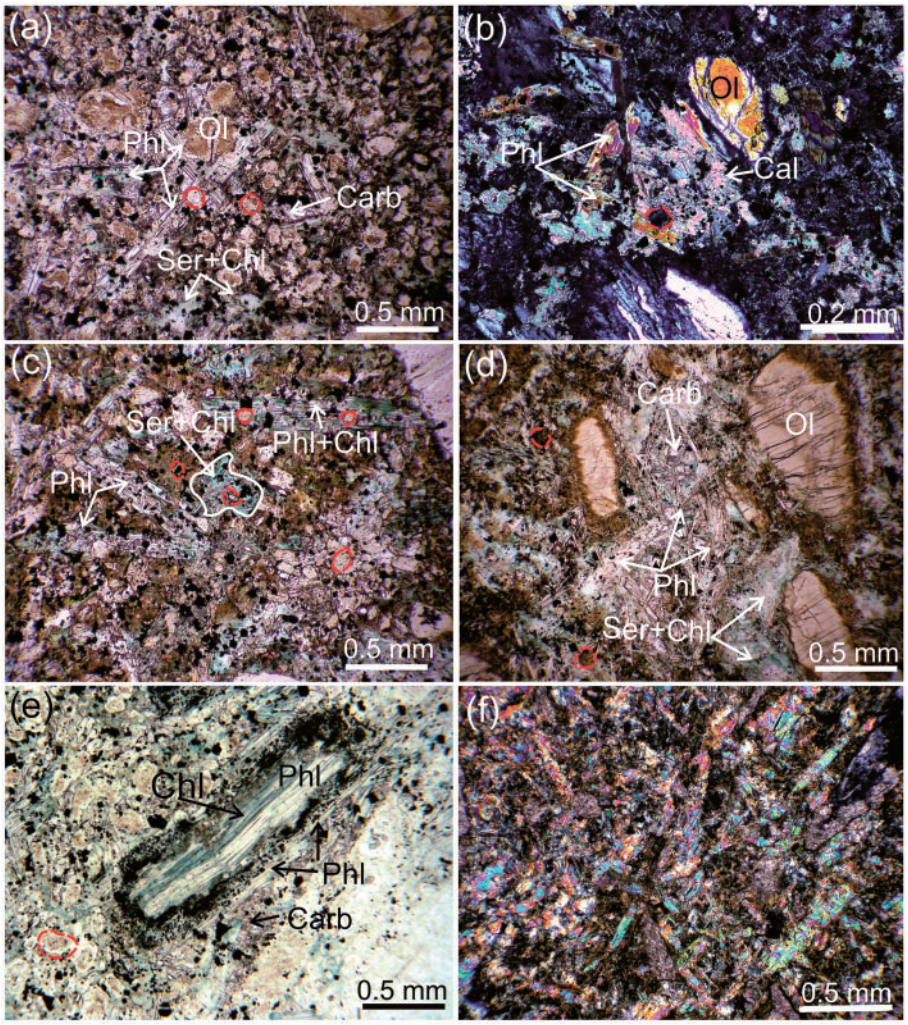

Fig. 6. Microscopic textures in HK1–2. (a) Poikilitic phlogopite (Phl) with spinel and serpentinized monticellite inclusions in a groundmass comprising monticellite (red dashed outline) and olivine (Ol) pseudomorphed by serpentine, serpentine and chlorite pools (Ser + Chl) with spinel inclusions and carbonate. (b) A general view of HK1 groundmass under crossed polars: fresh olivine, poikilitic phlogopite, serpentine, and poikilitic calcite (Cal). (c) A general view of an HK1–2 groundmass with abundant cross-cutting, elongate, poikilitic phlogopite with chlorite alteration, enclosing spinel and serpentinized monticellite. Note the dominant brown serpentine with relic monticellite shapes (red dashed outline), enlarged light colour monticellite pseudomorphs enclosed by phlogopite, and serpentine and chlorite pools with serpentinized monticellite and spinel inclusions. (d) A partly assimilated granitoid replaced by light colour serpentine, phlogopite, chlorite and carbonate, in an HK1–2 groundmass comprised of brown serpentine with rare relic monticellite pseudomorphs. Phlogopite has an elongate, needle-like cross-sectional shape and non-poikilitic texture. Serpentine and chlorite pools occur adjacent to the assimilated granitoid. (e) Macrocrystal phlogopite surrounded by magnetite rim in an HK2. Chlorite along cleavage planes is pseudomorphing ~50% of the phlogopite. Note the poikilitic phlogopite overgrowing the macrocryst and the carbonate pools in the groundmass comprised of light colour monticellite pseudomorphs and chlorite. (f) An HK2 groundmass under crossed polars, showing abundant cross-cutting elongate poikilitic phlogopite with rare spinel inclusions.

In HK5-6, the multiphase phyllosilicates are predominant (Fig. 7a–f), and phlogopite only occasionally has a poikilitic texture (Fig. 7a; Supplementary Data Fig. S3). Starting from HK4 and further closer to granitoid contacts, serpentine also becomes pseudomorphed by a multiphase phyllosilicate. All intermediate transitions are observed between the isotropic serpentine pseudomorphs after olivine and the multiphase phyllosilicate, which gradually develops perfect cleavage, greyish colour, and a higher birefringence optically resembling mica (Figs 7a–f, 8e, f; Supplementary Data Figs S3–S5). The multiphase phyllosilicate pseudomorphing serpentine after olivine appears dark in hand specimens, blending in with the colour of the groundmass and giving an impression that olivine is missing.

To summarize, the phlogopite mineralogy changes in proximity to granitoid in the following ways: (1) the total amount of phlogopite increases from HK1 to HK4 and then decreases from HK4 to HK5–6 as it is progressively replaced by multiphase phyllosilicates; (2) from HK1 to HK3, phlogopite transitions in shape from elongate poikilitic with inclusions of serpentinized monticellite and spinel to short prismatic tabular (with or without a rim with spinel inclusions) (Table 1; Fig. 8a, b; Supplementary Data Figs S2–S3).

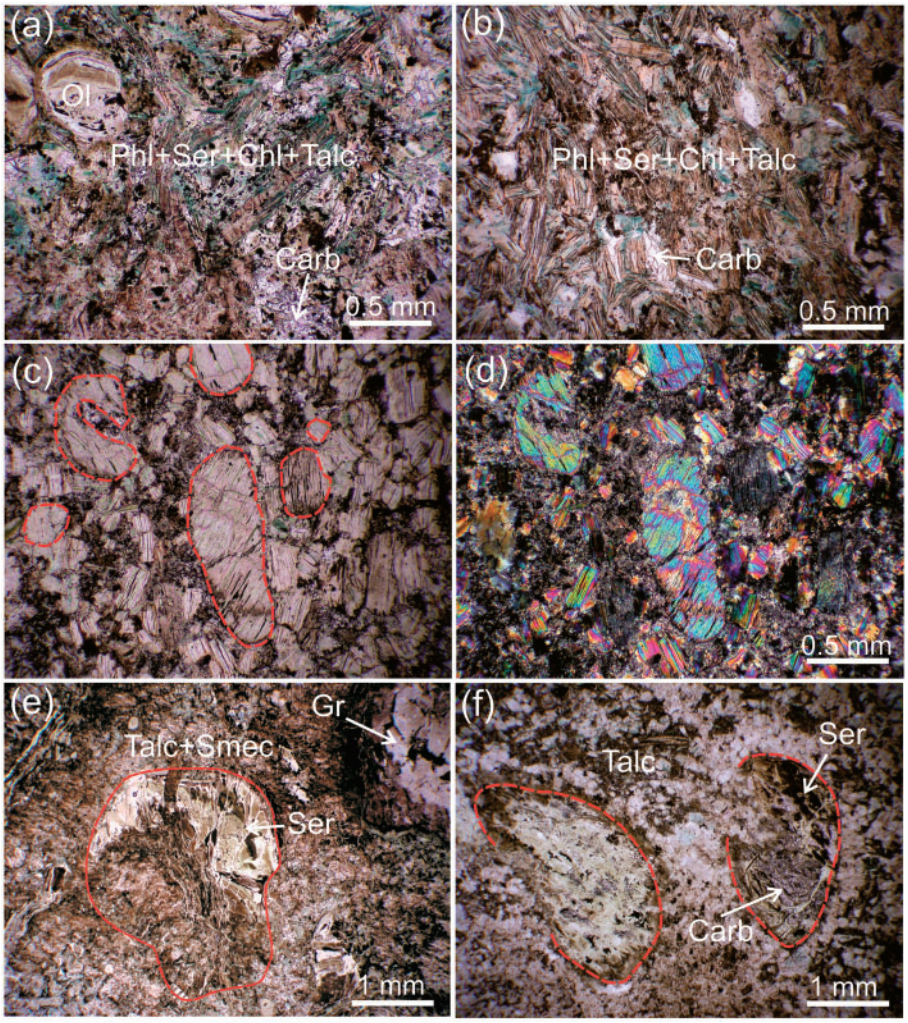

Fig. 7. Microscopic textures in HK5–6. (a) A general view of an HK5 groundmass comprising multiphase phyllosilicates: talc, chlorite, serpentine, and elongate poikilitic laths suggesting altered phlogopite. (b) Multiphase phyllosilicates in an HK6 groundmass with rare carbonate pools. (c) An image of an HK6 with serpentinized olivine and monticellite (red dashed outlines) pseudomorphed by multiphase phyllosilicates. Note that olivine preserves its original shapes while most of the monticellite grains change to a tabular shape. (d) Same image under crossed polars. (e) An olivine macrocryst (red dashed outline) pseudomorphed by serpentine (top half) and multiphase phyllosilicates (bottom half) which replace most of an HK6 groundmass. Altered granitoid xenolith (Gr) in the top right corner. (f) Image of a typical HK6 comprising phyllosilicates (dominantly talc) with relic olivine (red dashed outlines) pseudomorphed by serpentine.

COUNTRY-ROCKS IN CONTACT WITH KIMBERLITE

The *in situ* granitoid along the contact is brecciated, impregnated by multiple mm-size kimberlite veins (Fig. 2, sample A02179; Supplementary Data Fig. S9) and appears green or grey, chloritized and serpentinized, in contrast to the pink unaltered granitoid 0·5–2 m away from the contact. The latter is represented by tonalite in our analyses (55–60 vol % plagioclase, 25–30% quartz, 1–5% biotite, 1–2% hornblende, 1% titanite and apatite). Closer to the contact with the kimberlite, the tonalite transitions to altered tonalite, where plagioclase is replaced by mica and chloritized biotite, and intensely altered tonalite composed of serpentinized plagioclase, chlorite, phlogopite and calcite in varied proportions, with relatively abundant titanite and apatite (Supplementary Data Fig. S9). In contrast, the contact between the kimberlite and the metavolcanics remain unaltered and free of kimberlite veins.

Granitoid xenoliths are abundantly included in the kimberlite, where their content increases from 0·5 % in HK1 to 10–15% in HK6 (Table 1). Granitoids occurring as xenoliths shows diverse alteration at their contacts with kimberlite. The xenoliths are generally more strongly assimilated and altered in HK1, but the extent of the assimilation varies significantly, even within a single rock type. For example, GRK, similar to HK3–6 (Figs 4c, d, 5a, b), contains round, assimilated granitoid clasts that are almost indistinguishable from the kimberlite matrix (white dashed line in Fig. 5c), but also subangular to shard-like, less altered granitoid with light pinkish colours preserving the original texture (Fig. 5c). The

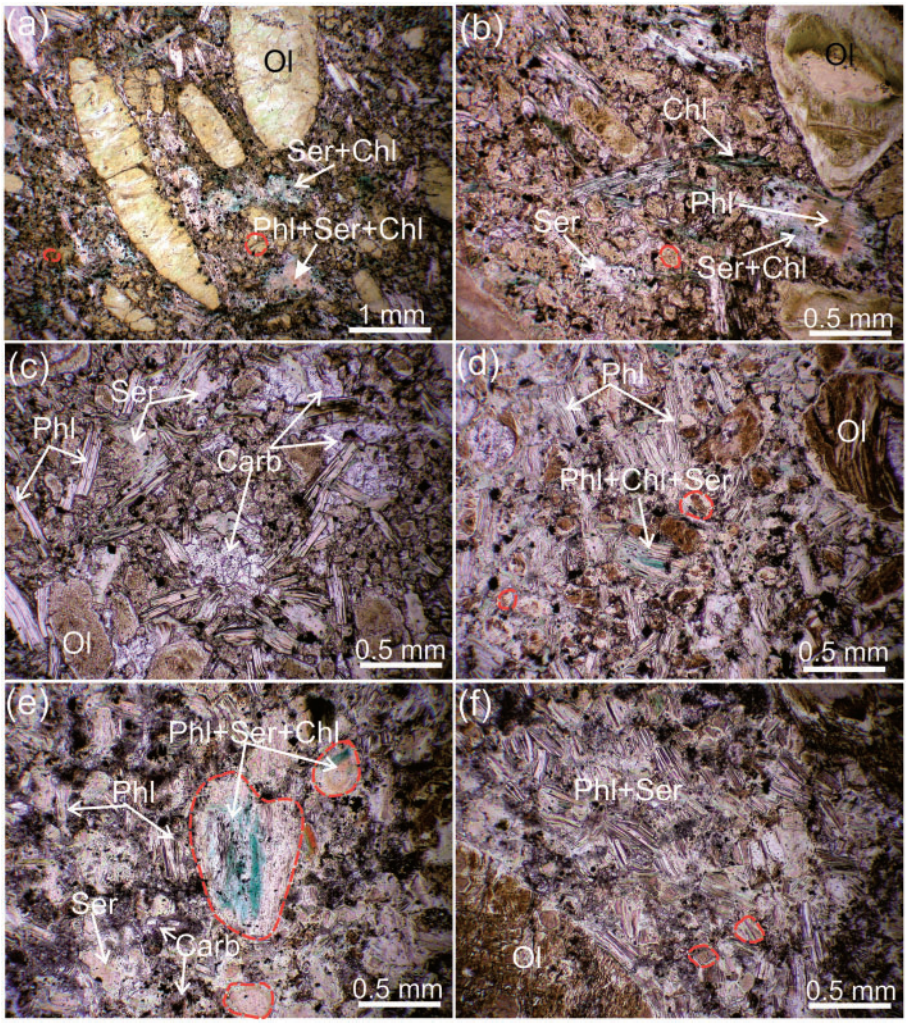

Fig. 8. Microscopic textures in HK3–4. (a) View of an HK3 comprised of serpentinized olivine macrocrysts, and a groundmass with abundant serpentinized monticellite (red dashed outlines) pseudomorphed by brown serpentine, elongate phlogopite enclosing spinel, and serpentine and chlorite pools with brown cores resembling the tabular phlogopite. (b) An HK3 groundmass comprised of olivine and monticellite pseudomorphed by serpentine, rare elongate poikilitic phlogopite, chlorite and serpentine pools. Note a brown tabular phlogopite (Phl) with serpentine rim enclosing spinel. (c) An HK3 groundmass comprised of tabular phlogopite, olivine and monticellite pseudomorphed by serpentine and carbonate pools. Tabular phlogopite crystallizes adjacent to the carbonate pools. (d) An HK4 groundmass comprised of altered tabular phlogopite, and olivine and monticellite (red dashed outlines) pseudomorphed by brown serpentine. Note the high abundance of phlogopite and the low abundance of monticellite pseudomorphs. (e) Olivine and monticellite pseudomorphs replaced by serpentine, chlorite and phlogopite in a highly serpentinized HK4–6 groundmass with rare relic serpentinized monticellite, and carbonate. Phlogopite is much less abundant than serpentine and carbonate. (f) An HK4–6 groundmass comprised of multiphase phyllosilicates. Light colour serpentine preserves rare relic monticellite shapes (red dashed outlines).

wide-ranging degrees of assimilation and alteration suggest a variable extent of interaction between the granitoid and the kimberlite, probably due to the variable residence time of the clasts in the kimberlite magma. Partly assimilated granitoid xenoliths show a consistent pattern of mineralogical zoning, whereby chlorite in the interior of the xenolith is surrounded by serpentine and phlogopite in the outermost zone of the xenolith (Figs 5d, c, 9a, b, d, e). In HK1, most xenoliths appear as diffuse patches of serpentine and carbonate (Fig. 9f).

The metavolcanic xenoliths do not show any evidence of assimilation, but are surrounded by thin zones rich in poikilitic phlogopite (Figs 3d, f, 5d).

KIMBERLITE ZONING AROUND GRANITOID XENOLITHS

The presence and abundance of granitoid xenoliths control mineralogical and textural changes in the kimberlite at a small scale, analogous to the zoning observed from the dyke center to the dyke margin (HK1 to HK6). Halos several centimeters wide develop everywhere around altered granitoid xenoliths (Fig. 9a). The halos are best developed around more altered xenoliths. Within these halos, the kimberlite grades from HK1 to HK2–5 (or from HK3 to HK4–6) at the contact with the xenoliths. Phlogopite increases in abundance closer to xenoliths and grows either perpendicular or

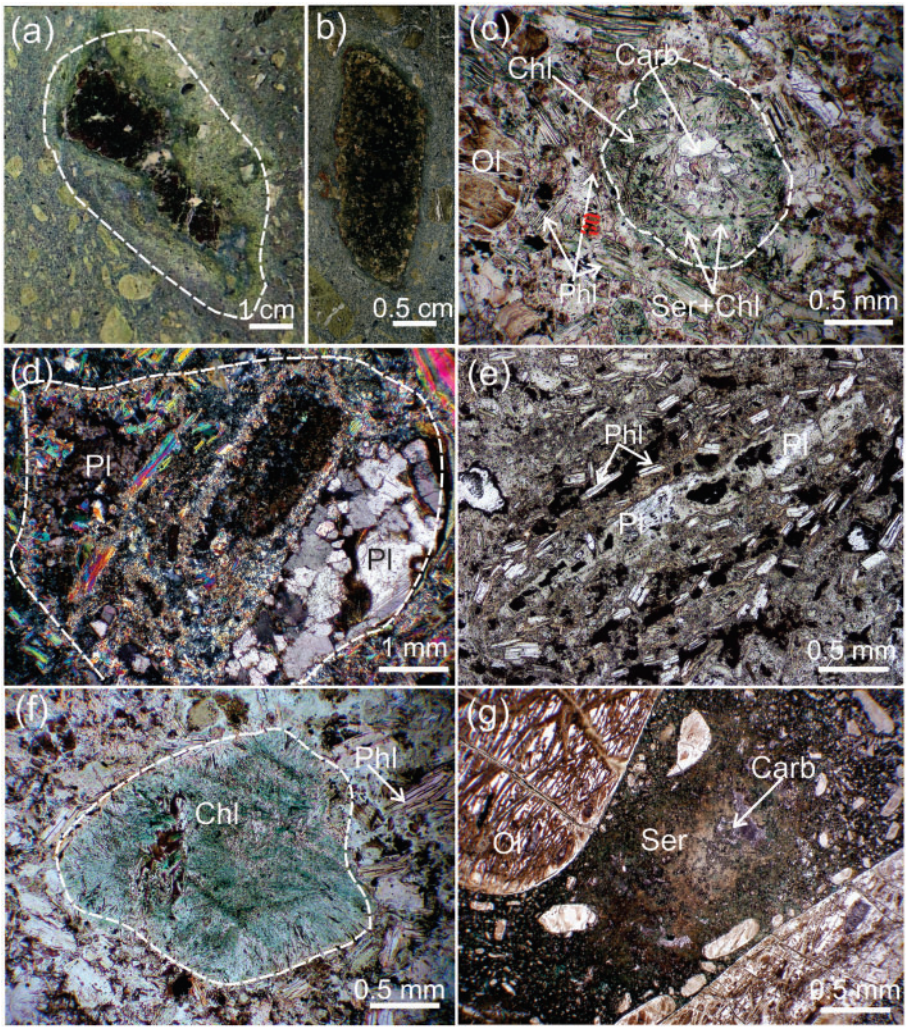

Fig. 9. Photomicrographs showing textures of the granitoid-kimberlite interaction. (a) Slab of HK4 with a moderately altered and assimilated granitoid xenolith. The dark green and white colours of the xenolith manifest development of chlorite and carbonate. Inside a light halo around the xenolith (white dashed outline) serpentine pseudomorphs after olivine are altered to phlogopite. (b) Detail of a granitoid xenolith in HK4, with moderate alteration to serpentine and a relic original texture, surrounded by a thin halo almost devoid of olivine and rich in phyllosilicates. (c) Assimilated granitoid xenolith (white dashed outline) replaced by chlorite, phlogopite and carbonate in the central part, altered phlogopite, serpentine and chlorite in the groundmass. Note rare relic serpentinized monticellite (red outline) and olivine pseudomorphed by serpentine. (d) Moderately altered granitoid xenolith (white dashed outline) preserves plagioclase, but is partially replaced by phlogopite and dark chlorite-bearing cryptocrystalline material. (e) Shard-like altered granitoid xenolith with relic plagioclase (Pl), surrounded by a halo of short prismatic phlogopite growing parallel to the clast margins. (f) Assimilated granitoid xenolith (white dashed outline) replaced by chlorite that crystallized from the margin inward in a groundmass comprised of amorphous serpentine with relict shapes of monticellite. (g) A distinct carbonate-rich domain enclosed by serpentine and devoid of olivine and monticellite pseudomorphs indicates the location of granitoid xenolith assimilation in HK1.

tangential to the xenolith outlines (Fig. 9b, d, e). Orange phlogopite pleochroism is more pronounced around xenoliths. In some zoned phlogopite crystals, this pleochroism is restricted to the margins overgrowing colourless cores. Serpentine pseudomorphs after olivine and monticellite are replaced by multiphase phyllosilicates (see below) only in the vicinity of assimilated granitoid (Fig. 9a, b, d, Supplementary Data Figs S4–S5). Where the zone of phlogopitization cross-cuts olivine pseudomorphs, only parts of the crystals are transformed to multiphase phyllosilicates and distorted in shape, while the remaining part of the pseudomorph stays as serpentine (Fig. 7e, f).

IDENTIFICATION OF PHYLLOSILICATES

In the course of petrographic and mineralogical examination of the rocks, we discovered a major mismatch between the optical and electron microprobe (EMP) identification of sheet silicates. More than 60% of all analysed 'phlogopite' grains are submicroscopic mixtures of several phyllosilicates. Analyses of these 'phlogopites' were not stoichiometric and on a Ba–K plot (Fig. 10a) define a wide field deviating towards the low-Ba side from the 1: 1 or 1: 2 Ba–K (cpfu) anticorrelation typical for kimberlitic phlogopites (Kopylova *et al.*, 2010) and carbonatitic micas (Ibhi *et al.*, 2005). All compositions not on these Ba–K trends have been

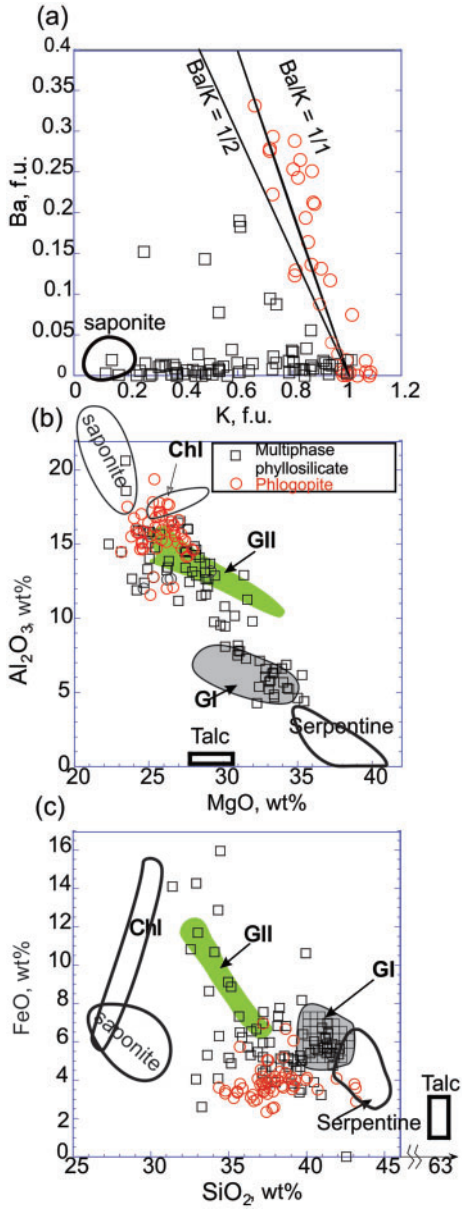

Fig. 10. Compositions of phlogopite compared with multiphase phyllosilicates. (a) Ba *vs* K (cations per formula units) of all minerals analysed as 'phlogopite'. (b) Al_2O_3 *vs* MgO (wt %), (c) FeO *vs* SiO_2 (wt %). Analyses of pure kimberlitic phyllosilicates are for chlorite (Kopylova & Hayman, 2008), clinochlore (Bailey, 1988), serpentine (Stripp *et al.*, 2006; Kopylova *et al.*, 2010), saponite (White *et al.*, 2012), and talc (Stripp *et al.*, 2006). Fields labeled GI and GII are multiphase phyllosilicates replacing olivines in the Venetia kimberlite and consisting of 50–80% lizardite with 20–50% smectite and 60–80% chlorite and 20–40% lizardite, respectively (Stripp *et al.*, 2006). Plot (a) shows lines with 1/2 and 1/1 Ba and K cation units observed in kimberlite phlogopite (Mitchell, 1986).

designated as 'multiphase phyllosilicates' below. X-ray diffraction studies are needed to determine correctly the mineralogy of these samples.

Powder diffraction analyses (Tables 2–3) done at two laboratories demonstrated a good match and identified several types of serpentine (lizardite-1 T, lizardite-2 H, clinochrysotile 2Mc1), chlorite, clinochlore-2 A, talc-2 M, phlogopite and biotite, saponite, dolomite and calcite in bulk specimens and in individual grains. Even in relatively fresh rocks such as HK1, lizardite is the most abundant sheet silicate, and phlogopite is subordinate to it. Clinochrysotile is observed only in HK1–4. Talc is more common in HK3–6 rock types than in HK1–2. Sheet silicates with high birefringence and perfect cleavage, replacing serpentine after olivine macrocrysts, are either pure talc or talc-lizardite mixtures (Table 3). Many optically identified groundmass phlogopite grains in HK1 rock types are lizardite (Table 3). Comparison of the compositions of these multiphase phyllosilicates with the compositions of phyllosilicate minerals common in other kimberlites showed that the mixtures contain significant serpentine, with less abundant chlorite and minor talc (Fig. 10). The mixtures retain a major proportion of the phlogopite component, as suggested by their K_2O abundances, which always exceeds 4 wt % (Table 4).

Phlogopite-lizardite intergrowths may be analogous to altered phlogopite with finely interlayered serpentine reported from the Frank Smith kimberlite (Sharp *et al.*, 1990). Phlogopite alteration, as observed using transmitted electron microscopy, involves cleavage openings along (001), formation of 50 nm-thick lamellae of lizardite with (001) layers parallel to phlogopite, partial transformation of lizardite to chrysotile, folding and clay mineral formation (Sharp *et al.*, 1990). Many of these processes are also observed in altered phlogopite at Snap Lake.

MINERAL CHEMISTRY

Phlogopite

The morphology and texture of different phlogopite types (Table 1; Fig. 11) correlate well with their compositions (Table 4; Figs 11–12). Large euhedral macrocrysts are distinctly low in BaO and Al_2O_3 (Fig. 12a, b). The rims of these crystals poikilitically enclose serpentinized monticellite and spinel, the same minerals found in long laths of poikilitic phlogopite (Fig. 6e). The rim of macrocrysts have compositions identical to poikilitic phlogopite. The latter are Ba-rich, while low in K_2O and TiO_2, and high in Al_2O_3. Zoning in these poikilitic phlogopites is extremely variable and complex. Backscattered electron images often show a resorbed, low-BaO core that could be a relic of macrocrystal phlogopite, or a relic of hybrid phlogopite that grew on assimilated granitoid (Fig. 11c; Supplementary Data Fig. S1). The rims overgrowing the resorbed cores, on average, are Ba-rich, but show a change from zones with increasing BaO, to zones with the opposite pattern (Fig. 12a). The highest BaO contents of 10–12 wt % occur only in poikilitic rims of hybrid phlogopite (Fig. 11c). Tabular, short, prismatic phlogopite has markedly lower BaO and higher FeO, TiO_2 and K_2O than poikilitic phlogopite. The tabular phlogopite is generally homogeneous (Fig. 11e–g), and only 10 out of 400 thin

Table 2: X-ray diffraction results for bulk Snap Lake samples

Mineralogical zone	Sample Number	Significant abundance	Moderate abundance	Minor to Moderate abundance	Minor abundance	Very minor abundance
HK1	PA100511		Lizardite		Dolomite, Saponite-15A	
HK2	PA105011		Clinocrysotile–2Mc1		Phl–1M, Lizardite, Chlorite	
HK2	PA106511		Lizardite, Clinocrysotile–2Mc1	Clinochlore, Calcite		Quartz
HK3	PA099311		Lizardite		Phl–2M1, Dolomite	
HK4	PA110911		Lizardite	Talc	Phl, Dolomite, Clinochlore	
HK4	PA103311		Lizardite		Phl, Talc	Clinochlore–1M1b
HK4	PA103711		Lizardite, Talc–2M		Phl, Calcite, Clinochlore	
HK5	PA106111			Lizardite, Phl	Dolomite, Clinochlore–1MIIb	
HK5	PA102511		Lizardite	Saponite–15A	Phl–2M1, Dolomite, Talc–2M	
HK6	PA112611	Lizardite		Talc, clinochlore		Phl–3T
HK6	PA104711			Dolomite	Phl–1M, Talc, Lizardite	
GRK	PA106211	Talc–2M		Phlogopite	Clinochlore–1M1a	
GRK	PA107911			Biotite–1M	Talc, Clinochlore–2A, Clinocrysotile–2Mc1, Quartz	Calcite
GRK	PA108011		Clinochlore–2A, Albite		Phl–1M, Quartz	
GRK	PA106611	Quartz			Clinochlore, Calcite	

Phl: phlogopite.

Table 3: Powder X-ray diffraction on individual grains of sheet silicates

Mineralogical zones	Sample Number	Textural position	Minerals
HK1	AO2155	Poikilitic Phl	Lizardite–1T + calcite
HK1	AO2155	Phl macrocryst with magnetite rim	Phl + brown millerite
HK3	AO2119	High birefringence mineral with cleavage replacing serpentine pseudomorphs after Ol macrocrysts	Talc–2M
HK3	AO2119	Tabular Phl in groundmass	Phl–1M + Talc–2M
HK4	AO2170	High birefringence mineral with cleavage replacing serpentine pseudomorphs after Ol macrocrysts	Lizardite 2H
HK4	PA114011A	High birefringence mineral with veering cleavage and wavy shape occurring in vein	Talc–2M
HK4	PA114011A	High birefringence mineral with veering cleavage and wavy shape comprising 90% of the rock	Lizardite–1T+Talc–2M
HK6	AO1838	Colourless low-birefringent mineral with subgrains replacing serpentine pseudomorphs after Ol macrocrysts	Lizardite–1T
HK6	AO1838	Light brown mineral with veering cleavage replacing Phl in the groundmass	Lizardite–1T

sections were found to contain thin rims higher in Al_2O_3 and BaO (Figs 8a, 11b, d).

Phlogopites replacing serpentine or granitoid xenoliths have distinct shapes, and their compositions plot in the fields identified above (Fig. 12c, d). Phlogopite growing on or adjacent to partially digested granitoid clasts in HK1–2 is poikilitic, needle-like or short tabular (Fig. 6d) and matches the compositions of poikilitic phlogopite in HK1–2. The difference between this granitoid-related phlogopite and phlogopite away from the xenoliths can be observed on a cm-scale and relates to increasing BaO (Fig. 12a, c). Phlogopite replacing and growing in haloes of partially digested granitoid in HK3–6 is short and tabular, plotting in the 'Tabular' compositional field (Fig. 12). Phlogopite pseudomorphs after serpentine replacing olivine and monticellite are identical in composition to high-Ti tabular phlogopite (Fig. 12c, d).

Other minerals

Olivine macrocrysts contain 91–92% forsterite (Fo). They may be slightly zoned, with more magnesian rims (from $Fo_{91.7}$ core to $Fo_{92.5}$ rim), or with a uniform composition (Table 4, Supplementary Data Table S2 (EST2)). Olivine microphenocrysts show more compositional heterogeneity and are either identical in composition to macrocrysts, or more ferrous (Fo_{87}).

The groundmass carbonate occurring in the only two samples with fresh olivine is represented by calcite, with up to 0·2 wt% SrO, up to 0·3 wt% BaO and < 2 wt% MgO (Table 5). In all other samples of HK1–2, the groundmass carbonate is dolomite (Kopylova *et al.*,

Table 4: Compositions of representative phlogopite, olivine and spinel in Snap Lake kimberlite

Mineral/ mineralogical zone	Grain, texture and location	Core or rim	SiO_2 wt%	TiO_2 wt%	Al_2O_3 wt%	Cr_2O_3 wt%	FeO Total wt%	MnO wt%	MgO wt%	Na_2O wt%	K_2O wt%	BaO wt%	F wt%	NiO wt%	Total wt%
Phlogopite															
HK1	poikilitic Phl lath	core	35·31	0·24	17·84		3·07	0·05	25·26	0·07	7·06	8·73	1·17		98·81
HK1	poikilitic Phl lath	rim	36·39	0·75	16·83		3·10	<MDL	25·47	0·05	7·78	7·54	1·17		99·09
HK3	tabular Phl	core	37·95	1·71	15·82		3·94	0·07	24·18	0·15	10·11	0·61	0·38		94·92
HK3	tabular Phl	rim	39·13	0·94	15·16		6·06	<MDL	24·56	0·14	9·71	0·46	0·52		96·76
HK6	secondary Phl after serpentine	core	41·19	0·49	5·22		6·16	<MDL	33·06	0·13	4·65	0·06			90·96
HK6	secondary Phl after serpentine	rim	38·13	0·99	7·51		6·82	<MDL	30·96	0·15	4·30	<MDL			88·85
HK6	mix of Phl, serpentine, chlorite and talc	core	39·76	0·93	6·60		6·40	<MDL	33·55	<MDL	2·93	0·58			90·76
Olivine															
HK1 with fresh Ol	macrocryst	core	41·00				8·13	0·09	50·15					0·46	99·82
Spinel															
HK1–3	groundmass grain	core	0·46	3·00	3·75	52·17	26·04	0·64	11·33						98·52
HK3–6	groundmass grain	core	0·47	3·37	5·89	54·66	19·89	0·39	13·73						99·21

Blanks, not analyzed, <MDL, below detection limit.

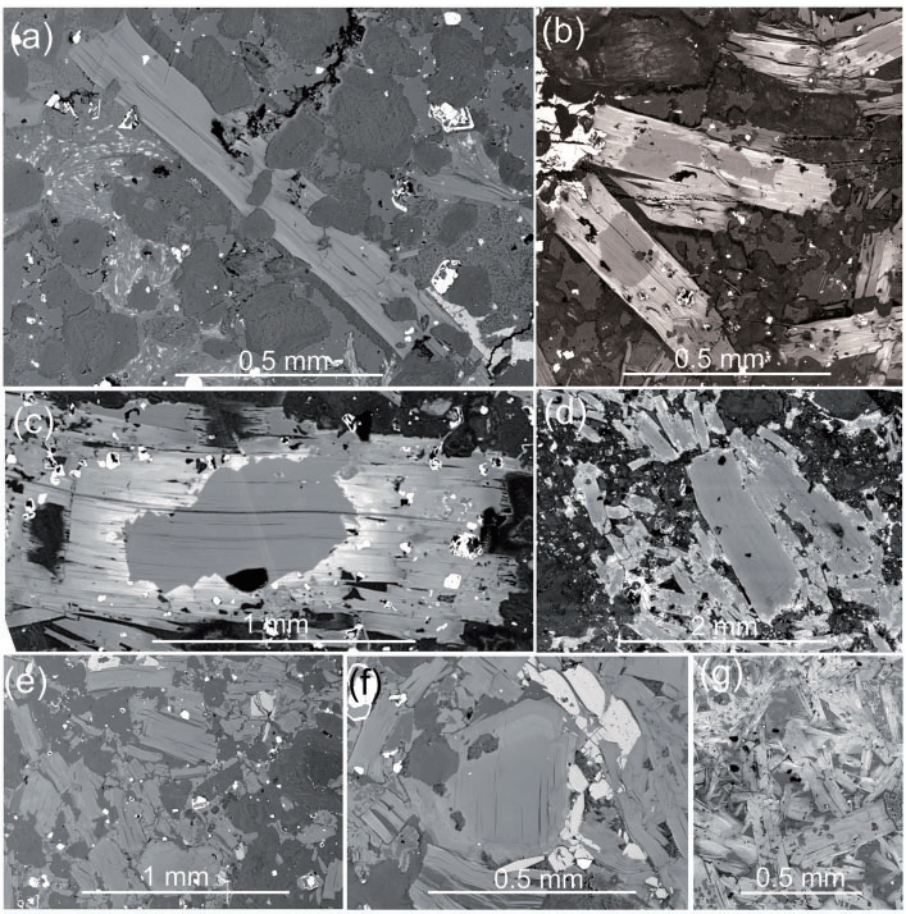

Fig. 11. Backscattered secondary electron images of phlogopite. (a) A lath of poikilitic phlogopite with inclusions of serpentinized monticellite in HK1. (b) Complexly zoned poikilitic phlogopite in HK2–3, showing a resorbed low-Ba core and a poikilitic overgrowth without inclusions of serpentinized monticellite. Here and in all photographs the brighter colour of phlogopite marks its high Ba content. Note that the overgrowth becomes lower in Ba towards the rim. (c) A complexly zoned phlogopite macrocryst in HK3, with a resorbed low-Ba rim and a high-Ba poikilitic overgrowth (with spinel but without serpentinized monticellite inclusions) in which Ba decreases rimward. (d) A rare example of tabular phlogopite with an outer rim rich in Ba in HK4. (e), (f) and (g) Homogeneous tabular phlogopite common in HK4–6.

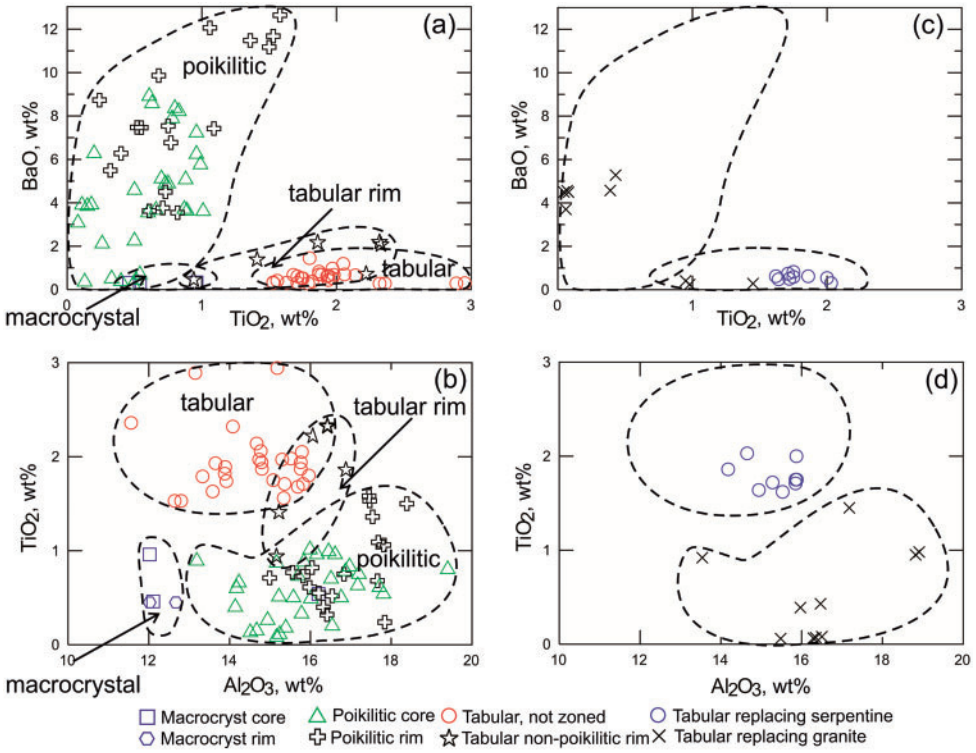

Fig. 12. Compositions of different textural types of phlogopite grouped according to their growth stages. (a) BaO *vs* TiO_2 (wt %), (b) TiO_2 *vs* Al_2O_3 (wt %). Fields outline the most common compositions of Phl with the corresponding texture and morphology. Field labelled 'Macrocrystal' includes analyses of macrocryst and phenocryst cores. Field 'Poikilitic' includes analyses from long poikilitic laths and rims of macrocrysts with inclusions of spinel and monticellite, as well poikilitic rims on other types of phlogopite. Field 'Tabular' includes analyses from cores of tabular grains and unzoned tabular grains. Field 'Tabular rim' encompasses rims of zoned tabular phlogopite. In (c) and (d) secondary and hybrid phlogopites are superimposed on the compositional fields 'Tabular' and 'Poikilitic' copied from (a) and (b).

2010). In all HK3–6 samples, calcite crystals occur in rhombic or subhedral discrete crystals and in multiple veins. The morphology of the groundmass calcite crystals is typical of secondary carbonate occurring in kimberlite (Kopylova & Hayman, 2008). In addition, the carbonate veins crosscutting pseudomorphed olivine macrocrysts attest to the secondary, post-emplacement origin of the calcite.

The spinel-group mineral is titanian magnesiochromite (Table 4, Supplementary Data Table S2 (EST2)), which plots on the magnesian ulvospinel trend typical of Group I kimberlites (Fig. 13). Spinel core compositions are identical in all mineralogical zones (HK1-6) and all fall in the main mode of low-Ti groundmass spinel previously documented in Snap Lake (Fig. 13). The spinel cores are rimmed by magnetite – magnesian ulvospinel solid solution minerals or rutile. Ti-magnetite rims have a Mg-rich (8-11 wt % MgO) composition with a considerable content of Al_2O_3 (2–4 wt %) and MnO (~1 wt %). Rutile is rich in Fe_2O_3 (2–8 wt %).

Perovskite is identified exclusively in the two HK1 samples with fresh olivine. The perovskite grains look pristine, with well pronounced zoning mimicking the present grain shapes, but all the analyses returned low totals (Table 5, Supplementary Data Table S2 (EST2)). We ascribe this deficiency, which may reach ~8 wt %, to the presence of water in altered porous perovskite, as Energy-Dispersive Scans did not indicate any missing elements. The formula of the perovskite is $(Na_{0.05}Sr_{0.01}Ca_{0.83}\ La_{0.03}Ce_{0.06})_{0.98}\ (Ti_{0.91}\ Al_{0.01}Nb_{0.04}\ Fe_{0.09})_{1.05}O_3$ indicating the presence of 5 mol% lueshite $NaNbO_3$ and 9 mol% Fe-loparite ($REEFeO_3$). The formula also reflects a 0·02 cpfu deficit of cations in the A-site, and the corresponding 0·05 cpfu excess of B-site cations. Perovskite rims are significantly poorer in Fe, Nb, La, Ce, and richer in Ca, Sr and Ti.

Apatite is rich in F (2–3·5 wt %) and Sr (~1 wt %; Table 5) and does not show any correlation of its composition with the grain habit of prismatic, radially clustered, poikilitic, or non-poikilitic grains. However, apatite crystallized next to digested granitoid clasts or on the site of assimilated granitoid shows increased concentrations of LREE (up to 2 wt %), but correspondingly lower Sr contents.

BULK-ROCK COMPOSITION

The Snap Lake kimberlite is petrographically classified as Group I, as it originally contained monticellite (Mitchell, 1986). Geochemically, however, it is more similar to Group II kimberlites on most plots (Fig. 14), reflecting an abundance of mica that is abnormally high for a Group I kimberlite. Moreover, the Snap Lake kimberlite stands out from the southern African Group II

Table 5: Representative compositions of groundmass carbonates, apatite and perovskite in the Snap Lake rock types

Mineral/ Rock type	Grain texture and location	TiO_2 wt%	Al_2O_3 wt%	FeO_{tot} wt%	MnO wt%	MgO wt%	CaO wt %	Na_2O wt%	F wt %	SrO wt%	P_2O_5 wt%	La_2O wt%	Ce_2O wt%	Nb_2O wt%	Total wt%
Carbonate															
HK1 with fresh Ol	Sr-rich calcite in groundmass			0·25	<MDL	0·07	56·25	0·49		0·19					
HK1 with fresh Ol	Sr-rich Mg-bearing calcite in groundmass			0·80	0·07	2·63	52·28	0·28		0·25					
HK2	Sr-free calcite			0·47	0·57	0·42	55·01	<MDL		<MDL					
HK3	Sr-free calcite in vein and granite replacement			0·35	0·36	0·35	55·43	<MDL		<MDL					
Apatite															
HK6	poikilitic grain in radial cluster			0·06			54·18	0·20	3·13	1·92	42·10	0·12	<MDL		101·70
HK6	poikilitic grain in radial cluster, next to granite			0·08			53·94	0·26	2·05	1·07	39·81	0·65	1·01		98·88
HK6	prismatic grain next to granite			0·14			51·89	0·17	2·92	1·10	39·98	0·76	0·94		97·92
HK2	non-poikilitic			0·15			53·50		2·49	1·97	42·15	<MDL	<MDL		100·26
Altered perovskite															
HK1 with fresh Ol	groundmass grain/core	46·93	0·35	3·93		0·09	29·71	0·85		0·43		2·58	6·08	3·09	94·03
HK1 with fresh Ol	groundmass grain/rim	53·65	0·06	1·45		0·04	35·68	0·56		2·01		0·34	0·48	1·53	95·80

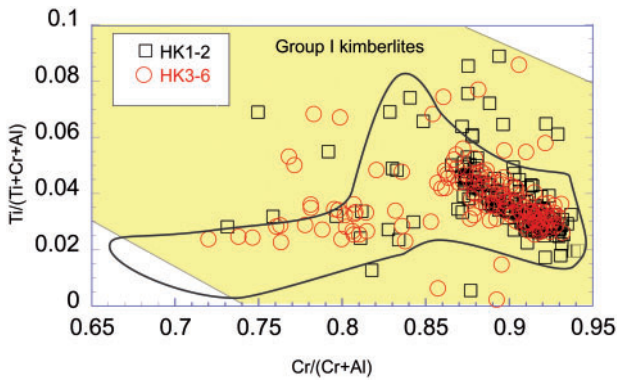

Fig. 13. Plot of Ti/(Ti + Cr + Al) *vs* Cr/(Cr + Al) cation ratios for Snap Lake spinels. Yellow band is a field of spinel compositions for Group I kimberlite (Mitchell, 1986). The field with a thicker black outline shows the compositions of 90% of Snap Lake spinels as reported in Kopylova *et al.* (2010). The larger field with a thinner outline includes all the Snap Lake spinels (Kopylova *et al.*, 2010).

kimberlites, which are inherently low in CaO, by its even lower CaO (Fig. 14c) and P_2O_5 (Kopylova *et al.*, 2010) contents. Despite plotting together with Group II kimberlites in most major element diagrams, Ba–Nb concentrations classify Snap Lake as Group I. The kimberlite falls below the Ba/Nb discriminant line (Fig. 14d) because its phlogopite, the major repository mineral for Ba in kimberlites (Mitchell, 1986), on average, is poorer in Ba than the typical kimberlite phlogopite, due to an overall high abundance of low-Ba tabular phlogopite.

Mineralogical and petrographic contrasts between the identified HK zones are accompanied by subtle and gradual changes in the bulk-rock composition (Table 6, Supplementary Data Table S3 (EST3)). HK1 has the lowest K_2O and SiO_2 and the highest Fe_{Total} (Fig. 15a, b) and MgO (Fig. 14a). The gradual increase in K_2O from HK1 to HK6 is not accompanied by a corresponding change in Na_2O, which stays constant (Table 6; Supplementary Data Table S3 (EST3)). The higher K_2O and SiO_2 contents in HK3–6 match the higher abundance of K-rich tabular phlogopite and the increased abundance of lizardite and smectite in the multiphase phyllosilicate (Table 1). The higher Fe_2O_3 and MgO in HK1 relates to higher modes of silicates and the lower modes of secondary carbonate and apatite; the latter is clearly observed in the higher Sr and P_2O_5 contents in some HK6 samples (Fig. 15d). The Rb-K_2O plot demonstrates distinct ratios of these elements for HK1, HK2–6 and for granitoid (Fig. 15c). The bulk composition of HK1 matches more closely the higher Rb/K ratio reported for kimberlites (line K on Fig. 15c; Mitchell, 1986), whereas kimberlites HK2–6 progressively deviate from HK1 towards the lower K/Rb ratios of the granitoids. The tight Rb-K_2O trend observed in the majority of HK2-6 zones plots on the trends leading to Ba-poor phlogopite (red arrow on Fig. 15c) and smectite (line S).

Table 6: Representative data of major and trace element geochemistry of the Snap Lake rock types

Rock Type	HK1	HK1	HK2	HK2	HK3	HK3	HK4	HK4	HK5	HK5	HK5/HK6	HK5/HK6	HK6	HK6	MVRK	GRK
Sample # A & PA	02112	02156	01190	01192	02158	02171	02132	02183	01854	01830	103611	104311	01166	01207	099611	106611
Major elements (wt %)																
SiO_2	36·24	35·78	32·34	36·19	36·15	35·27	35·36	36·18	38·46	33·49	38·83	35·69	41·13	40·94	39·74	57·67
TiO_2	0·66	0·73	0·58	0·69	0·82	0·88	0·80	0·74	0·74	0·50	0·81	0·69	0·65	0·58	1·02	0·56
Al_2O_3	3·06	2·48	2·52	3·83	2·97	3·36	3·13	2·61	4·14	2·30	4·93	3·54	2·83	2·09	12·86	4·07
Cr_2O_3	0·27	0·29	0·24	0·25	0·27	0·27	0·27	0·27	0·27	0·21	0·25	0·27	0·26	0·22	0·06	0·18
Total Fe as Fe_2O_3	7·60	8·67	7·82	8·30	6·50	7·44	6·83	7·57	7·67	6·45	7·44	7·49	7·14	5·82	12·26	4·48
MnO	0·13	0·14	0·10	0·14	0·12	0·13	0·11	0·15	0·10	0·13	0·11	0·15	0·12	0·13	0·19	0·09
MgO	30·22	31·74	33·54	29·38	28·95	28·80	29·72	30·74	31·69	25·07	28·81	30·73	28·45	21·23	17·21	9·98
CaO	4·80	3·83	4·18	3·99	6·74	6·31	5·57	5·36	2·49	11·80	2·36	3·09	3·88	11·37	4·91	9·48
Na_2O	0·08	0·05	0·04	0·04	0·05	0·02	0·04	0·03	0·03	0·05	0·09	0·07	0·05	0·19	0·85	0·06
K_2O	0·68	0·70	0·76	1·49	1·08	1·49	1·72	1·05	1·10	0·83	1·03	0·84	1·31	0·88	1·81	0·58
P_2O_5	0·61	0·59	0·06	0·54	0·88	0·35	0·77	0·58	0·33	0·15	0·51	0·49	0·23	0·61	0·19	0·95
LOI	15·00	14·30	17·40	14·60	15·00	15·00	15·10	14·20	12·60	18·60	13·70	15·70	13·50	15·20	8·30	11·40
Sum	99·54	99·53	99·76	99·53	99·61	99·45	99·59	99·60	99·74	99·76	99·03	98·87	99·71	99·47	99·49	99·54
Total C	1·11	0·86	1·91	1·38	1·60	1·45	1·37	1·11	0·64	2·66	0·62	0·97	1·52	2·74	0·11	1·92
Trace elements (ppm)																
Sc	13	12	11	13	14	14	13	12	12	10	13	12	12	9	38	10
Ba	2277	2134	904	2323	1396	2455	1982	1730	1051	748	1997	3873	1353	2123	706	1385
Co	67·1	65·9	53·7	66·3	183·6	92·1	71·3	99·5	48·9	88·1	59·8	71·4	80·8	72·8	60·7	19·3
Ga	5·3	3·9	5·0	5·0	5·1	6·2	4·9	5·8	13·7	5·1	9·2	4·9	4·1	2·2	14·9	8·6
Hf	2·3	2·7	1·9	2·4	2·5	3·1	2·5	2·9	2·3	2·0	3·4	2·6	1·6	2·3	2·0	2·4
Nb	163·6	203·8	160·3	200·7	234·2	296·8	217·0	203·9	219·2	126·5	275·5	191·7	144·6	177·7	45·4	202·3
Rb	69·5	58·1	50·6	95·7	57·7	89·1	90·9	58·8	59·3	42·5	80·8	87·3	65·9	77·4	50·5	38·6
Sr	486·7	397·2	57·3	380·2	289·0	207·7	241·7	205·4	104·9	128·6	340·4	363·3	82·5	228·0	367·9	381·0
Ta	12·1	13·2	10·0	11·2	13·1	14·6	11·3	13·0	13·4	8·6	14·5	12·4	12·2	9·9	2·2	8·8
Th	35·2	35·3	29·3	36·3	45·3	45·7	33·2	35·7	38·4	27·7	41·2	38·2	37·8	43·5	8·9	22·2
U	4·2	3·0	1·5	5·0	3·0	3·4	5·1	3·4	3·2	1·8	5·1	3·0	3·0	13·8	3·2	5·2
V	47·0	40·0	44·0	89·0	70·0	44·0	37·0	43·0	29·0	23·0	51·0	58·0	41·0	30·0	291·0	92·0
Zr	77·1	103·2	96·7	114·8	112·2	120·5	134·8	116·1	87·6	71·5	136·0	103·7	68·5	156·0	100·6	109·9
Y	10·7	8·6	15·2	12·6	15·3	13·2	11·5	9·9	6·4	15·8	9·9	11·0	6·8	34·4	20·5	14·2
La	148·4	212·9	141·7	96·7	161·4	211·8	122·8	179·7	77·5	135·3	392·0	264·0	86·4	306·5	41·0	93·3
Ce	254·7	370·6	234·8	183·9	283·9	538·0	238·4	310·5	141·2	215·9	619·3	409·2	153·8	493·2	78·4	150·1
Pr	23·43	33·28	23·0	19·3	26·2	58·8	23·8	30·0	14·0	20·9	53·0	33·4	15·6	46·7	7·4	15·4
Nd	73·5	99·6	74·2	61·0	81·4	196·3	76·9	96·8	44·2	66·6	157·4	98·0	46·4	136·1	24·6	51·0
Sm	9·51	10·15	10·0	9·2	11·4	20·1	9·9	12·2	5·2	8·9	14·9	9·6	6·4	15·8	4·0	7·5
Eu	2·4	2·4	2·6	2·5	3·0	5·1	2·4	2·8	1·2	2·3	3·0	2·2	1·6	4·1	1·2	2·0
Gd	6·9	6·9	7·6	7·0	8·4	12·2	6·4	7·6	3·4	7·1	7·2	5·5	4·5	12·5	3·9	5·7
Tb	0·7	0·6	0·9	0·8	0·9	1·0	0·6	0·7	0·4	0·7	0·7	0·7	0·5	1·5	0·7	0·7
Dy	3·0	2·5	3·5	3·8	4·0	4·0	2·4	2·8	1·4	3·3	2·7	2·7	1·8	6·8	3·5	2·9
Ho	0·4	0·3	0·4	0·5	0·5	0·5	0·3	0·3	0·2	0·4	0·4	0·4	0·3	1·2	0·8	0·4
Er	0·9	0·8	1·0	1·2	1·0	1·0	0·9	0·7	0·5	1·0	0·8	0·8	0·6	2·6	2·2	1·1
Tm	0·1	0·1	0·1	0·1	0·1	0·1	0·1	0·1	0·1	0·1	0·1	0·1	0·1	0·3	0·3	0·2
Yb	0·6	0·5	0·9	0·8	0·6	0·6	0·6	0·5	0·4	0·5	0·8	0·7	0·4	1·5	2·2	0·8
Lu	0·1	0·1	0·1	0·1	0·1	0·1	0·1	0·1	0·1	0·1	0·1	0·1	0·1	0·2	0·3	0·1
Cu	1·5	1·3	0·8	18·2	37·4	8·6	6·8	1·4	0·2	45·7	156·5	6·1	1·0	225·9	113·4	13·4
Pb	1·2	1·4	10·4	2·4	1·4	1·6	3·0	4·7	1·9	1·0	1·5	1·2	2·9	23·1	2·9	4·2
Zn	31·0	25·0	17·0	27·0	18·0	34·0	25·0	32·0	27·0	20·0	30·0	23·0	22·0	21·0	48·0	22·0
Ni	1069·9	1302·3	1065·8	960·9	781·3	1074·9	1214·2	1352·1	1079·3	865·3	969·0	1256·5	993·8	946·7	339·6	427·1

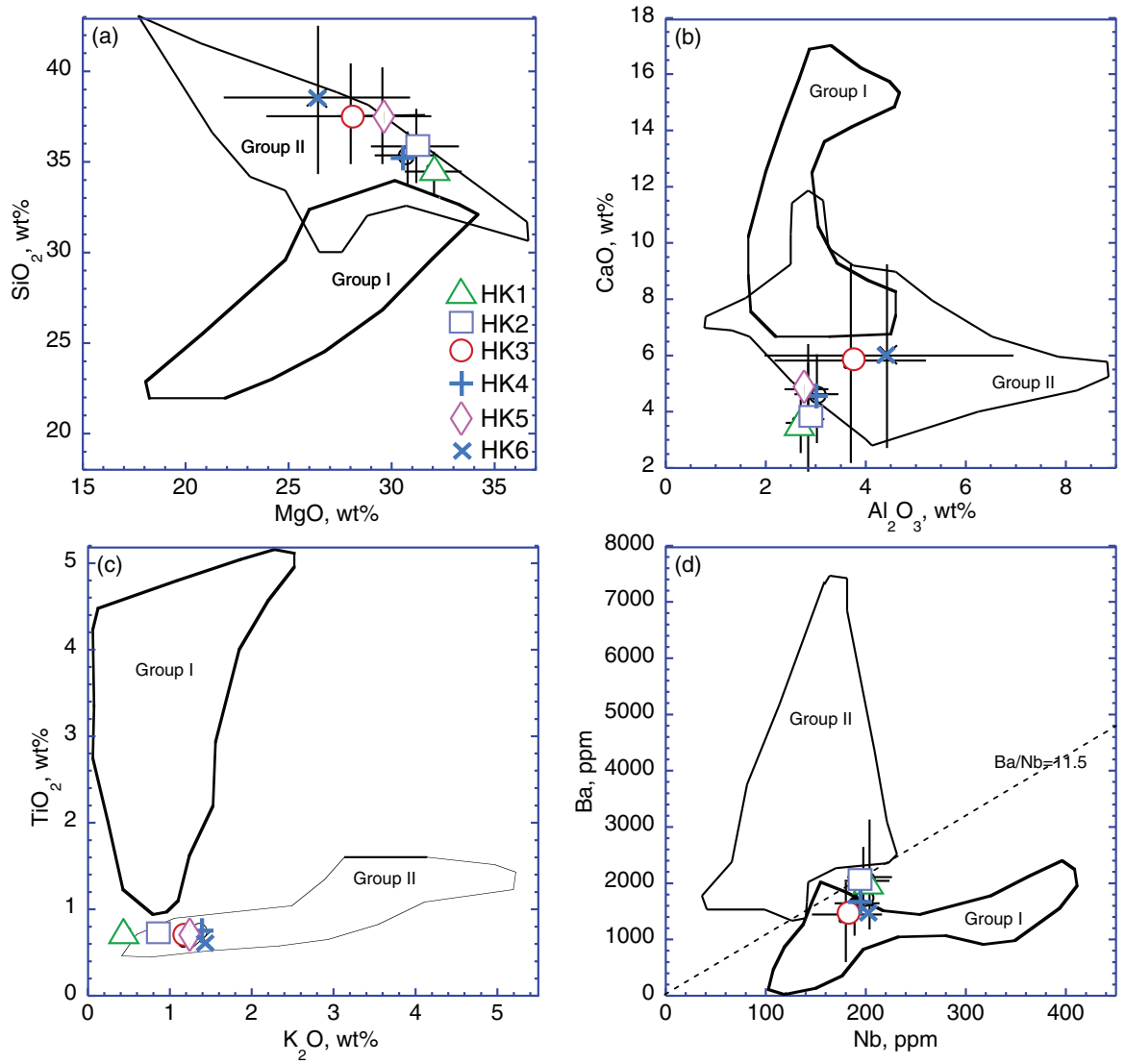

Fig. 14. Bulk composition of the Snap Lake kimberlite compared to South African Group I and Group II kimberlites (wt %). (a) SiO_2 *vs* MgO, (b) TiO_2 *vs* K_2O, (c) CaO *vs* Al_2O_3, (d) Ba *vs* Nb. Types of the Snap Lake kimberlite are plotted as average compositions with 1 standard deviation error bars. For the TiO_2 vs. K_2O plot, the error bars (0·2–0·5 wt % for K_2O and 0·1 wt % for TiO_2) are not shown. South African kimberlite compositions are from Becker & Le Roex (2006). The TiO_2–K_2O field excludes two outlying compositions of Group II kimberlites with abundant ilmenite megacrysts. A dashed line with the Ba/Nd=11·5 separates Group II and Group I kimberlites in (d).

As kimberlite facies change systematically away from the center of the dyke to the granitoid contact, a spatial profile (Fig. 2) can provide additional information on possible kimberlite-granitoid interaction. The profiles shown in Fig. 16 demonstrate how MgO and Ni decrease, whereas K_2O increases towards the contact with the host granitoid, i.e. from HK1 to HK2 to HK5 and HK6. The compositions of the rocks change smoothly and systematically and lack abrupt contrasts, as expected from magmas that belong to distinct separate batches. Abrupt jumps in the concentrations of CaO, Ba, Nb, Nd and Sr in kimberlites are superimposed on the gradual compositional changes, particularly at the contact with the granitoid where the kimberlites show pervasive post-emplacement carbonatization of the groundmass and carbonate veining.

The observed systematic gradual compositional profiles continue into the host granitoid. The granitoid away from the kimberlite dyke contains lower Mg, volatiles (expressed as LOI), P_2O_5, TiO_2, Nb and Ba, while showing higher SiO_2 and Na_2O (Fig. 16). The granitoid close to the contact shows an increase in REE, Nb, Ta, Th, U and Ni (Supplementary Data Figs S7–S8), elements that are inherently higher in kimberlites. The changes are partly caused by the more intense contact metasomatism of the granitoid, and partly by the development of 1–15 vol.% kimberlite veinlets in the brecciated granitoid in a 30 cm thick zone next to the contact.

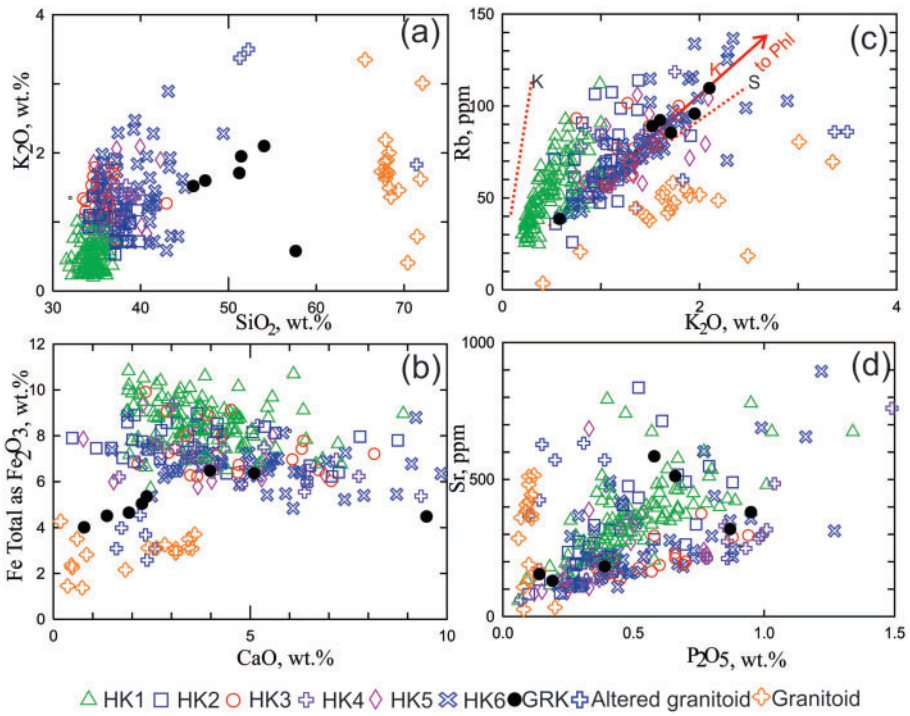

Fig. 15. Whole-rock compositions of kimberlite rock types. (a) K_2O *vs* SiO_2 (wt %), (b) Total Fe (as Fe_2O_3) vs CaO (wt %), (c) Rb *vs* K_2O (wt %), (d) Sr (ppm) *vs* P_2O_5 (wt %). All six recognized kimberlite zones and granitoid are labeled with different symbols. Superimposed on (c) are dashed red lines of K/Rb ratios for kimberlites (K) and smectite-rich rocks (S). Line K is based on Fig. 7·20 of Mitchell (1986). Line S is constrained by the trace element chemistry of smectite-rich sediments (Grizelj *et al.*, 2017). A red line with an arrow points to Ba-poor phlogopite as constrained by the data of Giuliani *et al.* (2016).

The composition of the granitoid in contact with the kimberlite does not resemble the bulk composition of the granitoid-rich kimberlite (GRK; Fig. 15), although both rocks are essentially composed of granitoid and kimberlite. Compositional fields of GRK, including trace elements and REE, are comparable in all geochemical plots to the fields of HK5–6 (Fig. 15; Supplementary Data Figs S7–S8).

The trace element contents in the kimberlite and granitoids (Table 6, Supplementary Data Table S3 (EST3); Supplementary Data Figs S7–S8) are discussed in the supplementary files.

DIAMOND CONTENT

The diamond content and diamond size frequency of HK1–2 and HK3–6 rocks are very similar, as illustrated by the log-probability plot of Fig. 17 of the diamond size frequency in HK1–2 and HK3–6 rocks despite their distinct textures. Both distributions are quite fine-grained and overlay each other. The curves follow a lognormal type distribution typical of other kimberlite diamond deposits. The number of microdiamonds recovered per kg for each of the microdiamond sieve classes (referred to as stone density of microdiamonds) from the two rock groups is also remarkably similar. HK1–2 has 13·5 microdiamonds per kg sampled (stones/kg) and HK3–6 has 13·9 stones/kg. For coarser-grained (microdiamonds larger than 212 μm/kg) sieve classes, the stone density of the two rock groups is almost identical at 1·4 stones larger than 212 μm/kg. As diamond size distributions are usually distinct to individual kimberlite units within a kimberlite body (Chapman & Boxer, 2004; Bush, 2010), the overall similarity in diamond content and diamond size frequency of HK1–2 and HK3–6 rocks supports the argument that the Snap Lake dyke crystallized from a single batch of magma. Differences in lithology and texture emerged syn- and post-emplacement by interactions with the country-rocks.

DISCUSSION

Shallow crystallization and subsolidus alteration in reaction with deuteric volatiles

The initial bulk composition of the Snap Lake magma was more calcic than its present composition, possibly similar to typical Group I kimberlites. Shallow crystallization formed groundmass spinel, perovskite and monticellite, often included in poikilitic phlogopite. The poikilitic phlogopites grew from stagnant, almost fully crystallized magma as evidenced by their random, cross-cutting orientation (Fig. 6a–c, f; Supplementary Data Fig. S1; Kopylova *et al.*, 2010; Gernon *et al.*, 2012). The progressive overgrowth of macrocrystal cores by poikilitic phlogopite resulted in the common compositional pattern characteristic of kimberlite phlogopite zoning globally, i.e. the core-to-rim decrease in K and increase in Ba, Al and F at a low Ti and Cr contents (Mitchell, 1986; Reguir *et al.*, 2009). A crude positive correlation between BaO and TiO_2 observed in poikilitic

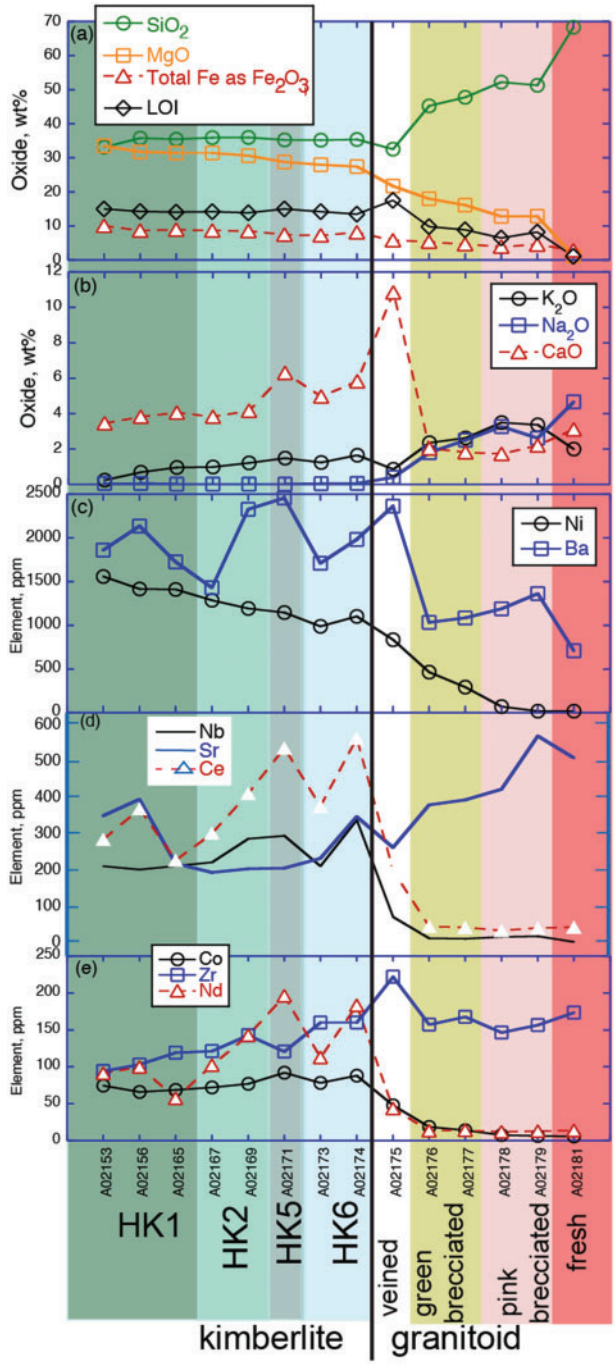

Fig. 16. Chemical profiles along the UG-12-1196 systematic sampling profile. (a) Profiles for SiO_2, MgO, Total Fe and LOI (wt %). (b) Profiles for K_2O, Na_2O and CaO (wt %). (c) Profiles for Ni and Ba (ppm). (d) Profiles for Nb, Sr and Ce (ppm). (e) Profiles for Co, Zr and Nd (ppm). The background in different colours marks the various rock types labeled at the bottom.

phlogopite (Fig. 12a) is common in kimberlite mica (Reguir *et al.*, 2009). Incorporation of Ba into the crystal lattice of phlogopite at the expense of K occurs only at low pressure (Righter & Carmichael, 1996) and thus is a hallmark of the crustal *in situ* crystallization.

The Ca-depleted character of the kimberlite, in our opinion, relates to serpentinization and other subsolidus deuteric reactions, which significantly affected the Snap Lake kimberlite. Since perovskite and primary calcite occur only in the freshest olivine-bearing HK1, and both phases are absent from all other HK1–2, we conclude that the serpentinization of olivine and monticellite, and the alteration of perovskite and calcite are related. One of the key factors in these replacement processes may be the acidic fluid regime controlled by deuteric CO_2. The olivine + calcite assemblage is not stable in the presence of an H_2O-CO_2 fluid and transforms to hydrous silicate + dolomite at T ~500°C at 100 MPa (Fig. 7 of Tracy & Frost, 1991) i.e.

$$2Mg_2SiO_{4(Ol)} + CaCO_3 + 2CO_{2(fluid)} + 2H_2O_{(fluid)} = Mg_3Si_2O_5(OH)_{4\ (Srp)} + CaMg(CO_3)_2 \quad (1)$$

Dolomitization of calcite is thus expected in all kimberlites where exsolved magmatic CO_2+H_2O linger in contact with freshly-crystallized olivine and calcite. This process operates through a release of Mg cations from olivine during its replacement by serpentine (Stripp *et al.*, 2006) and reaction of the Mg with calcite. Perovskite, fresh in only two HK1 samples, is also unstable in CO_2-rich magmas and fluids and is eventually replaced by patchy domains of Ti-rich minerals, including titanates (Mitchell & Chakhmouradian, 1998; Chakhmouradian & Mitchell, 2000). At Snap Lake, mild alteration is observed in texturally pristine, yet compositionally modified, perovskite with leached Ca and the corresponding excess of B-site cations (Table 5). In the more altered Snap Lake kimberlite with serpentinized olivine, perovskite is also replaced by monazite and rutile (Ogilvie-Harris *et al.*, 2009). The *in situ* replacement of the calcic minerals calcite, perovskite, monticellite, common to many kimberlites, has developed to such a major extent at Snap Lake that this Group I kimberlite has a much lower bulk CaO content than even Ca-poor Group II kimberlites (Fig. 14c). This low CaO content in HK1 is the base level for the special geochemical analysis (isocon analysis) discussed below.

Our conclusion on the link between deuteric CO_2, dolomitization and serpentinization is supported by the mineralogy of fresh hypabyssal kimberlites elsewhere (Armstrong *et al.*, 2004). These authors postulated that 'formation of dolomite is a localized overprint', based on: (1) the absence of dolomite in magmatic laths of carbonate; (2) the presence of dolomite in carbonate segregations only in kimberlites where monticellite is completely serpentinized and spinel is altered into atoll textures; and (3) the variable presence of dolomite in drill core at the scale of 2–3 m. Furthermore, the higher CO_2 content of dolomite-bearing kimberlites (Fig. 12 of Armstrong *et al.*, 2004) provides one more argument for the requisite presence of deuteric CO_2 for dolomite formation. The common calcite replacement with dolomite in kimberlites attests to the effectiveness of deuteric volcanic gases for olivine serpentinization and sequestering the newly available Mg as dolomite.

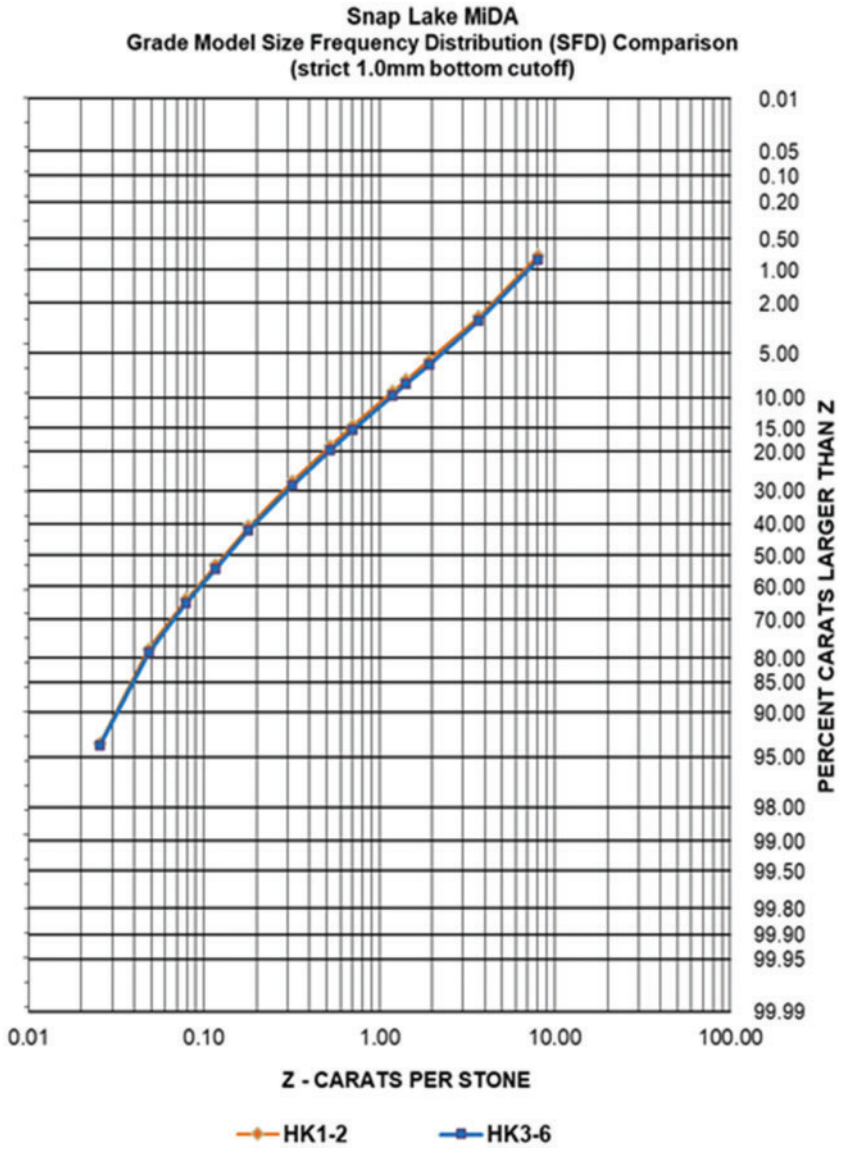

Fig. 17. Diamond Size frequency distribution for Snap Lake kimberlite rock groups HK1–2 and HK3–6.

Superimposed on in the dolomitization and serpentinization processes at the Snap Lake dyke is the development of secondary calcite in post-emplacement veins and throughout the groundmass along the dyke margins in HK3–HK6.

The effects of kimberlite-granitoid interaction

We attribute the unusual Si-rich and Ca-poor bulk chemistry of the Snap Lake kimberlite and its mineralogy rich in sheet silicates to interaction with the host granitoid, the evidence for which is:

- The absence of the more altered rock types (HK3–6) in the kimberlite intruding metavolcanic rocks, irrespective of the dyke thickness.
- A progressive increase in the abundance of phlogopite and phlogopite-bearing multiphase phyllosilicates from the center of the dyke towards the granitoid-kimberlite contact.
- A correlation between modes of tabular phlogopite and multiphase phyllosilicates with the dyke thickness in the granitoid-hosted dyke: the thinner the dyke, the higher the modal abundance of phyllosilicates.
- The development of phlogopite and multiphase phyllosilicate grains around granitoid clasts and their absence around other types of xenolith.
- The orientation of phlogopite perpendicular or parallel to the granitoid clast outlines (Fig. 9c, e).
- Replacement of olivine and monticellite pseudomorphs by multiphase phyllosilicates exclusively at the contact between kimberlite and granitoid.

Our conclusion on the central role of country-rock granitoid in the development of the distinct mineralogy and chemistry of the Snap Lake kimberlite contradicts

previously published studies of the dyke (Field *et al.*, 2009; Gernon *et al.*, 2012). These authors described HK6 kimberlite in the dyke selvages as olivine-poor kimberlite (OPK), distinct from olivine-rich kimberlite (ORK), which corresponds to HK1. They attribute the mineralogical and textural differences between the two varieties of the kimberlite to crystallization from two separate batches of the kimberlite magma, emplaced consecutively. However, pervasive alteration has severely changed the texture of the rock, making an accurate determination of its olivine content difficult to impossible, especially when rock types are mapped from underground photographs (Gernon *et al.*, 2012). In our opinion, any attempt to ascribe the origin of HK6 (OPK) solely to a magmatic process is incorrect. This rock type, which contains only phyllosilicates (phlogopite, serpentine, chlorite and talc) does not match the bulk composition of any volcanic rock, and its mineralogy certainly does not match either Group I or Group II kimberlites. This unique rock can only be 'hybrid' and recrystallized.

Quantitative assessment of granitoid contamination *versus* metasomatism in isocon analysis

The compositional center-to-margin changes in the Snap Lake dyke relate to its interaction with granitoid. This interaction could include several processes such as granitoid incorporation, magma hybridization due to assimilation of granitoid xenoliths and contact metasomatism. To distinguish between these processes, we deployed an improved (Guo *et al.*, 2009) isocon analysis (Grant, 1986) to portray the metasomatic gains and losses of elements in kimberlites and country-rocks. The method requires scaling whole-rock compositions in such a way that an immobile element is normalized against the value in the protolith. We designated the average composition of HK1 as the kimberlite protolith, and the average fresh granitoid (tonalite with $K_2O < 2$ wt %) as the granitoid protolith. The isocon approach is fundamentally related to Pearce element ratio analysis (Pearce, 1968; Russell & Nicholls, 1988). The method restores extensive relationships between rock compositions and thereby overcomes the problem of closure inherent in variation diagram analysis (Chayes, 1962). Inspection of all element ratios supported Zr or Hf as the best choices for an immobile element in the kimberlites, and Zr, Hf, or Ti in the granitoids. We thus chose Zr as the immobile element in our isocon analysis.

To portray extensive relationships as deviations from the protolith, we subtracted (translated) the Zr-normalized protolith composition from all Zr-normalized compositions. The average HK1 composition was subtracted from all kimberlites, and the average tonalite was subtracted from all granitoids. In the kimberlites, we further accounted for variability arising from average granitoid assimilation/contamination. In the granitoids we accounted for physical contamination by microveins of

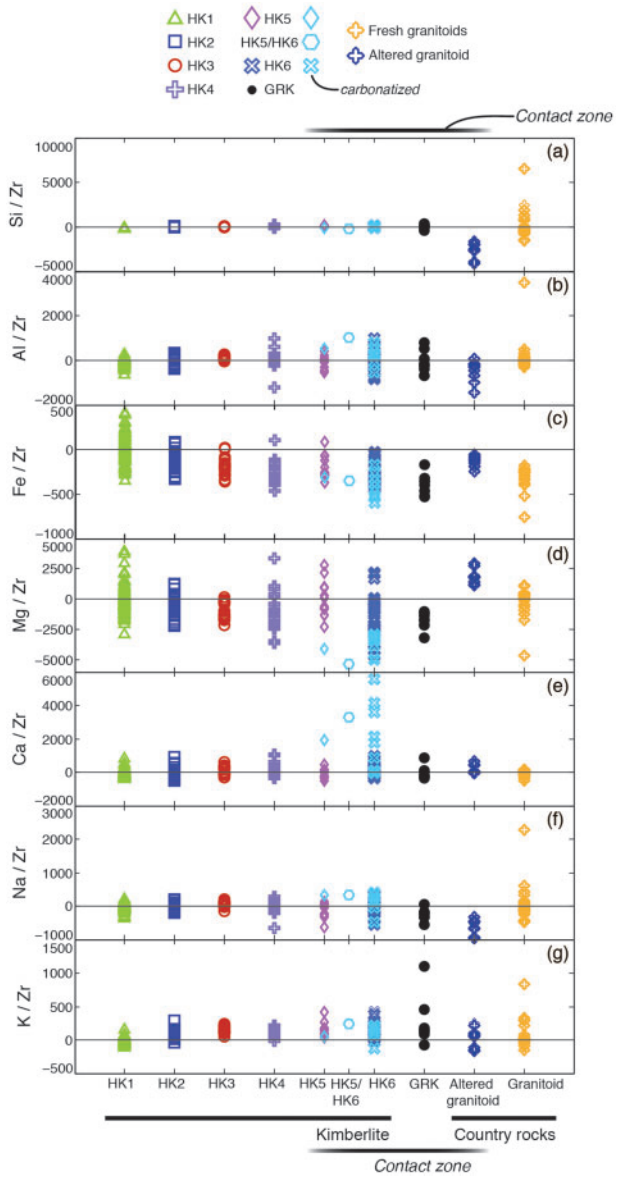

Fig. 18. Stoichiometric changes in rock compositions arising principally from metasomatism of kimberlites and granitoid country-rocks. Changes are calculated from Zr-normalized rock compositions (Guo *et al.*, 2009) using the updated isocon method, as well as projection procedures to account for physical mixing between the main lithologies. (a) Si/Zr, (b) Al/Zr, (c) Fe/Zr, (d) Mg/Zr, (e) Ca/Zr, (f) Na/Zr, (g) K/Zr.

kimberlite (average HK1). We treated the principal variation in GRK as mixing of average HK1 and average granitoid. In each case, we adjusted for these processes by projecting the scaled and translated rock compositions onto the pertinent composition (i.e. average HK1, average tonalite), and then subtracted the amount of the component captured by the projection. This procedure determines the maximum amount of the scaled and translated rock composition that the process could explain. Removing this component provides an estimate of the effects of metasomatism. However, variability related to heterogeneity of the intruding magma and the variable composition of the granitoid host-rocks affects

the assessed amount of incorporated xenoliths. In the current modeling we chose the assumptions on the fresh composition of the granitoids and the initial variability of the kimberlite that returns the minimum magnitude of metasomatism. Under these conditions, the constrained amount of incorporated and assimilated xenoliths match the petrographic estimates, but more sophisticated geochemical modeling is necessary to accurately quantify the contributions of xenolith contamination *vs* metasomatism. Irrespective of the initial assumptions, the more xenolith-rich units (HK4–6) trend to higher average granitoid content.

The resulting plot of Fig. 18 presents rock compositions as secondary metasomatic stoichiometric gains (positive) or losses (negative) from the protolith. Hypabyssal kimberlites and GRK show little evidence for metasomatic changes in Si, whereas altered granitoids are distinctly Si-depleted compared to their protolith. Lack of metasomatic changes to Si in the kimberlite units indicates that contamination and assimilation of country rocks could accommodate enrichment in Si, rather than metasomatic transfer. Mixing of average granitoid with average HK1 does not account for Si variability in the altered granitoid, and metasomatic losses of Si are required.

The kimberlites and GRK show evidence for both gains and losses of Al, and losses of Mg and Na. More altered kimberlites and GRK demonstrate higher metasomatic gains of Al and higher losses of Fe and Mg. Large ranges of Fe and Mg in even the freshest kimberlite lithologies likely correspond to varied initial olivine mode and changes attending early serpentinization, which mobilizes Fe in other ultramafic systems (e.g. Douville *et al.*, 2002; Hilchie, 2017). Altered granitoids lost Al and Na, gained Mg, Fe and Ca.

GRK is very similar in metasomatic change to the kimberlites at the contact (HK5, HK6). Even though GRK formed due to brecciation of granitoid in kimberlite, the isocon analysis confirms that the GRK composition cannot be explained by simple physical mixing. Formation of GRK is impossible without significant metasomatism.

Alkalies and Ca show consistent behavior in all lithologies of kimberlite and granitoid. Ca is metasomatically added, similar throughout all kimberlite lithologies except for substantial gains in carbonatized samples. Similar to Ca, metasomatic changes in K tend to be positive in all lithologies of kimberlite and in most altered granitoids. Enrichments are greatest in GRK and the most altered hypabyssal kimberlites (HK5 and HK6). The ingress of both Ca and K are especially noticeable along dyke margins, indicating infiltration-assisted reactions. Sodium is uniformly depleted in all lithologies, rather than being complementary in the host-rock and in the intruded dyke.

Contamination by granitoid xenoliths

Enrichment of altered kimberlites HK3–6 in Si, and partly in Al relates to contamination by granitoid xenoliths. Isocon analysis suggests that these elements, together with others added metasomatically, enable the growth of phlogopite and multiphase phyllosilicates.

Contribution of granitoid contamination to the growth of poikilitic phlogopite is evidenced by the correlation of its mode with the abundance of granitoid xenoliths (Table 1) and identical compositional fields of poikilitic phlogopite and phlogopite replacing or growing adjacent to granitoid (Fig. 12a, b). The tabular phlogopite also grew from contaminated kimberlite magma, as suggested by the following observations. Firstly, the tabular phlogopite is constrained to the margins of the dyke, to HK3–6, which contain abundant granitoid. Secondly, tabular phlogopite has a Ti-rich composition, similar to phlogopite replacing serpentine pseudomorphs after olivine and monticellite, and the phlogopite replacing or growing in the haloes of granitoid xenoliths in HK3–6 (Fig. 12b, d), or in veins. High Ti and low-Ba cores in large tabular phlogopite with high Ba and low Ti poikilitic rims (Fig. 11c) may have grown on hybrid patches where granitoid was magmatically assimilated.

Multiphase phyllosilicates replacing poikilitic Ba-rich phlogopite, serpentine and tabular Fe- and K-rich phlogopite also resulted in part from addition of Si and Al supplied by granitoid xenoliths. The ultimate product of this replacement is a lizardite-rich, smectite-bearing rock, composed of warped grains of a multiphase phyllosilicate, with larger grains crystallized on sites of former olivine macrocrysts (Fig. 7c, d; Supplementary Data Fig. S4).

The granitoid assimilation may have started in the magma, but most of the xenolith digestion proceeded during a subsolidus stage, resulting in the growth of subsolidus phlogopite and a multiphase suite of phyllosilicates. Additional indirect evidence for a predominant low-T nature of the granitoid replacement in Snap Lake is its mineralogical and textural contrast to the Gahcho Kue kimberlite. At Gahcho Kue, the coherent kimberlite assimilated granitoid xenoliths at higher magmatic temperatures, as suggested by diopside coronas on the xenoliths and pseudomorphing pectolite (Caro *et al.*, 2004). Domains with such mineralogy (Supplementary Data Fig. S6) are rarely observed at Snap Lake, reflecting the predominance of subsolidus reactions that form metasomatic phyllosilicates.

Metasomatic reactions with local and distal element sources

All deviations from the 'zero' line on Fig. 18 relate to the metasomatic ingress or depletion of elements superimposed onto natural kimberlite heterogeneity, rather than to a physical addition of a contaminant as a xenolith or a vein. Three elements, Al, Fe and Mg, behave in the kimberlite and the host granitoid in a complementary fashion, indicating local, meter-scale, skarn-like transport. Aluminium was removed from the granitoid and added to the kimberlite. Mineralogically

this is expressed as replacement of feldspar by serpentine and carbonate, and crystallization of phyllosilicates in the kimberlite. The ingress of granitoid-derived Al to a limited distance inside the dyke was counteracted by the flux of Mg and Fe to the granitoid. This caused loss of serpentine and spinel from the kimberlite and formation of serpentine and chlorite in the altered granitoid.

Calcium, Na and K cannot be balanced on a local, several meter scale and require distal transport, i.e. the ingress of K and Ca and the removal of Na. Enrichments in Ca and K on both sides of the contact imply precipitation of Ca and K-bearing minerals in the metasomatized rocks. These minerals include multi-phase phyllosilicates, apatite, and carbonates in kimberlites, phlogopite and carbonate in granitoids near the contact, and sericite and apatite in distal granitoids. Universal losses of Na imply that the Na-undersaturated metasomatic fluid extracted Na by replacement of feldspars by serpentine and carbonate in granitoids and granitoid xenoliths. The extremely high influx of Ca to the often carbonatized HK5–6 may be partly sourced from CO_2-rich fluids that leached perovskite and monticellite and promoted subsolidus dolomitization of the kimberlite, Perhaps the balance of Ca removed from the dyke was mobilized to its margins and near-contact carbonate veins in both kimberlite and granitoid.

The juxtaposition of a carbonate-bearing rock against a felsic rock at a high temperature at Snap Lake is reminiscent of many other well-studied examples of such contacts. This kind of interaction has been documented in multiple occurrences of granite intrusions into sedimentary carbonates, where internal chemical potential gradients at the contact trigger meter-scale metasomatism developing through diffusion and fluid infiltration (Barton *et al.*, 1991*a*; Meinert *et al.*, 2005). The geochemical changes caused by this interaction depend on the composition of the silicate rocks and the temperature of the magma (Barton *et al.*, 1991*b*). Most broadly, potassic alteration in skarns is best developed in contact with granites, whereas mafic magmas rarely have skarns in contact with carbonates because of the diminished magmatic chemical activity of Si (Barton *et al.*, 1991*b*). In full correspondence with these patterns, we see the weak subsolidus secondary alteration of the kimberlite when it intrudes mafic metavolcanics, but an intense alteration at the granitoid-kimberlite contacts. Potassic alteration and large skarns form in contact with quartzo-feldspathic rocks only at higher temperatures (Einaudi *et al.*, 1981; Barton *et al.*, 1991*b*), 450-730°C (Atkinson & Einaudi, 1978; Pirajno, 2008). The temperatures of a shallow kimberlite magma (600-1000°C at 100 MPa, Kopylova *et al.*, 2007 and references therein) permit the high-temperature mobility of K and Si. The shorter range transport of Fe, Mg and Al and the more distal mobilization of alkalies and alkaline earth metals at Snap Lake is typical for observed and theoretical mobilities of elements in metasomatic processes (e.g. Dolejs & Wagner, 2008).

Our observations on the mobility of alkalies at Snap Lake contribute to the understanding of fenitization around kimberlites. Potassium and Ca were mobilized and participated in the fenitization, whereas the little Na available in the kimberlite was only removed, contributing to the scarcity of kimberlite-related sodic fenites.

CONCLUSIONS

The altered margins of the Snap Lake dyke could be considered a rare example of contact metasomatism superimposed on the carbonate-rich-intrusive protolith. The skarn-like process that affected the Snap Lake dyke, however, had its own 'quirk'— the intimate link with xenolith contamination. Kimberlites commonly have country-rock breccias at their contacts (Clement, 1982) and incorporate local wall-rock as xenoliths. If the country-rock clasts are reactive in the magma and are in contact with the kimberlite for an extended time, assimilation of the xenoliths ensues.

The Snap Lake dyke alteration highlights the potential of kimberlites to produce metasomatic zones when juxtaposed against felsic rocks. The zones are essentially kimberlite-felsic skarns enhanced by the assimilation and metasomatic alteration of granitoid xenoliths. Kimberlite geologists involved in resource modelling should especially be aware of the susceptibility of kimberlites to granitoid-induced hybridization and metasomatism that deceptively look like separate emplacement phases, which may mislead grade expectations.

ACKNOWLEDGEMENTS

AF and SK acknowledge the support from Snap Lake mine and geologists Kevin Gostlin, Julianna Benke, David Dudar, Jim Granville, Nick van Battum, Tim Holmans and Alan Joyce. Victor Toth from DBCI is thanked for performing the image analysis work. Jim Evans and Lee Groat (UBC) helped with sample preparation and interpretation of XRD analysis on thin sections. AF and SK are grateful to Anglo American and DBCI management for the support received to publish the data Nick Arndt, Andrea Giuliani, Jennifer Pell and Lucy Porrit are thanked for reviewing and improving the manuscript. Executive Editor Marjorie Wilson and Editorial Manager Alastair Lumsden are thanked for their continuous support during the revision and submission of the manuscript.

FUNDING

MGK and LK were able to work on this project due to an Natural Sciences and Engineering Research Council of Canada Discovery grant.

SUPPLEMENTARY DATA

Supplementary data for this paper are available at *Journal of Petrology* online.

REFERENCES

Armstrong, J. P., Wilson, M., Barnett, R. L., Nowicki, T. & Kjarsgaard, B. (2004). Mineralogy of primary carbonate-bearing hypabyssal kimberlite, Lac de Gras, Slave Province, Northwest Territories, Canada. *Lithos* **76**, 415–433.

Atkinson, W. W., Jr & Einaudi, M. T. (1978). Skarn formation and mineralization in the Contact Aureole at Carr Fork, Bingham, Utah. *Economic Geology* **73**, 1326–1365.

Bailey, S. W. (1988). Chlorites: structures and crystal chemistry. In: Bailey, S. W. (ed.) *Hydrous Phyllosilicates. Mineralogical Society of America, Reviews in Mineralogy* **19**, 347–403.

Barton, M. D., Ilchik, R. P. & Marikos, M. A. (1991a). Metasomatism. In: Kerrick, D. M. (ed.) *Contact Metamorphism. Mineralogical Society of America, Reviews in Mineralogy and Geochemistry* **26**, 321–349.

Barton, M. D., Staude, J.-M., Snow, E. A. & Johnson, D. A. (1991b). Aureole systematics. In: Kerrick, D. M. (ed.) *Contact Metamorphism. Mineralogical Society of America, Reviews in Mineralogy and Geochemistry* **26**, 723–847.

Becker, M. & Le Roex, A. P. (2006). Geochemistry of South African on- and off-craton, Group I and Group II kimberlites: petrogenesis and source region evolution. *Journal of Petrology* **47**, 673–703.

Bush, D. (2010). *An Overview of the Estimation of Kimberlite Diamond Deposits. The 4th Colloquium on Diamonds-Source to Use*. Johannesburg: The Southern African Institute of Mining and Metallurgy, pp. 73–84.

Caro, G., Kopylova, M. G. & Creaser, R. A. (2004). The hypabyssal 5034 kimberlite of the Gahcho Kue cluster, Southeastern Slave Craton, Northwest Territories, Canada: a granite-contaminated Group-I kimberlite. *The Canadian Mineralogist* **42**, 183–207.

Chakhmouradian, A. R. & Mitchell, R. H. (2000). Occurrence, alteration patterns and compositional variation of perovskite in kimberlites. *The Canadian Mineralogist* **38**, 975–994.

Chapman, J. G. & Boxer, G. L. (2004). Size distribution analysis for estimating diamond grade and value. *Lithos* **76**, 369–375.

Chayes, F. (1962). Numerical correlation and petrographic variation. *The Journal of Geology* **70**, 440–452.

Clement, C. R. (1982). A comparative geological study of some major kimberlite pipes in the Northern Cape and Orange Free State. Unpublished Ph.D. thesis. Cape Town: University of Cape Town, 431 pp.

Dolejs, D. & Wagner, T. (2008). Thermodynamic modeling of non-ideal mineral-fluid equilibria in the system Si-Al-Fe-Mg-Ca-Na-K-H-O-Cl at elevated temperatures and pressures: implications for hydrothermal mass transfer in granitic rocks. *Geochimica et Cosmochimica Acta* **72**, 526–553.

Douville, E., Charlou, J. L., Oelkers, E. H., Bienvenu, P., Jove Colon, C. F., Donval, J. P., Fouquet, Y., Prieur, D. & Appriou, P. (2002). The Rainbow vent fluids (36°14′N, MAR): the influence of ultramafic rocks and phase separation on trace metal content in Mid-Atlantic Ridge hydrothermal fluids. *Chemical Geology* **184**, 37–48.

Einaudi, M. T., Meinert, L. D. & Newberry, R. J. (1981). Skarn deposits. In: Skinner, B. J. (ed.) *Economic Geology 75th Anniversary Volume*. El Paso, Texas: The Economic Geology Publishing Company, pp. 317–391.

Ferguson, J., Danchin, R. V. & Nixon, P. H. (1973). Fenitization associated with kimberlite magmas. In: Nixon, P. H. (ed.) *Lesotho Kimberlites*. Lesotho National Development Corporation, Cape and Transvaal Printers Ltd, pp. 207–217.

Field, M., Gernon, T. M., Mock, A., Walters, A., Sparks, R. S. J. & Jerram, D. A. (2009). Variations of olivine abundance and grain size in the Snap Lake kimberlite intrusion, Northwest Territories, Canada: a possible proxy for diamonds. *Lithos* **112S**, 23–35.

Gernon, T. M., Field, M. & Sparks, R. S. J. (2012). Geology of the Snap Lake kimberlite intrusion, Northwest Territories, Canada: field observations and their interpretation. *Journal of the Geological Society* **169**, 1–16.

Giuliani, A., Phillips, D., Kamenetsky, V. S. & Goemann, K. (2016). Constraints on kimberlite ascent mechanisms revealed by phlogopite compositions in kimberlites and mantle xenoliths. *Lithos* **240–243**, 189–201.

Grant, J. A. (1986). The isocon diagram; a simple solution to Gresens' equation for metasomatic alteration. *Economic Geology* **81**, 1976–1982.

Grizelj, A., Peh, Z., Tibljaš, D., Kovačić, M. & Kurečić, T. (2017). Mineralogical and geochemical characteristics of Miocene pelitic sedimentary rocks from the south-western part of the Pannonian Basin System (Croatia): implications for provenance. *Studies Geoscience Frontiers* **8**, 65–80.

Guo, S., Ye, K., Chen, Y. & Liu, J. B. (2009). A normalization solution to mass transfer illustration of multiple progressively altered samples using the isocon diagram. *Economic Geology* **104**, 881–886.

Heaman, L. M., Kjarsgaard, B. A. & Creaser, R. A. (2004). The temporal evolution of North American kimberlites. *Lithos* **76**, 377–397.

Hilchie, L. (2017). Recovery of geochemical processes in komatiites using linear algebraic methods. Unpublished Ph.D. thesis. Vancouver: University of British Columbia, 171 pp.

Ibhi, A., Nachit, H. & El Abia, H. (2005). Titanium and barium incorporation into the phyllosilicate phases: the example of phlogopite-kinoshitalite solid solution. *Journal of Physique IV* **123**, 331–335.

Le Bas, J. M. (2008). Fenites associated with carbonatites. *The Canadian Mineralogist* **46**, 915–932.

Kopylova, M. G. & Hayman, P. (2008). Petrology and textural classification of the Jericho Kimberlite, Northern Slave Province, Nunavut, Canada. *Canadian Journal of Earth Sciences* **45**, 701–723.

Kopylova, M. G., Matveev, S. & Raudsepp, M. (2007). Searching for parental kimberlite melt. *Geochimica et Cosmochimica Acta* **71**, 3616–3629.

Kopylova, M. G., Mogg, T. & Scott Smith, B. H. (2010). Mineralogy of the Snap Lake Kimberlite, Northwest territories, Canada, and compositions of phlogopite as records of its crystallization. *The Canadian Mineralogist* **48**, 549–570.

Meinert, L. D., Dipple, G. M. & Nicolescu, S. (2005). World skarn deposits. In: Hedenquist, J. W., Thompson, J. F. H., Goldfarb, R. J. & Richards, J. P. (eds.) *The Economic Geology 100th Anniversary Volume*. Littleton, Colorado: Society of Economic Geologists, Inc. pp. 299–336.

Mitchell, R. H. (1986). *Kimberlites: Mineralogy, Geochemistry and Petrology.* New York: Plenum Press, 442 pp.

Mitchell, R. H. & Chakhmouradian, A. R. (1998). Instability of perovskite in a CO_2-rich environment: examples from carbonatite and kimberlite. *The Canadian Mineralogist* **36**, 939–951.

Ogilvie-Harris, R. C., Sparks, R. S. J., Field, M. & Gernon, T. M. (2009). The geochemistry of the Snap Lake kimberlite dyke, NW Territories, Canada: Phlogopite and spinel. *Eos Transactions American Geophysical Union* **90**(52), Joint Assembly Supplement, Abstract V33D-01.

Pearce, T. H. (1968). A contribution to the theory of variation diagrams. *Contributions to Mineralogy and Petrology* **19**, 142–157.

Pirajno, F. (2008). *Hydrothermal Processes and Mineral Systems*. Berlin: Springer Science & Business Media, Springer Netherlands, 1250 pp.

Reguir, E. P., Chakhmouradian, A. R., Halden, N. M., Malkovets, V. G. & Yang, P. (2009). Major- and trace-element compositional variation of phlogopite from kimberlites and carbonatities as a petrogenetic indicator. *Lithos* **112S**, 372–384.

Righter, K. & Carmichael, I. S. E. (1996). Phase equilibria of phlogopite lamprophyres from western Mexico: biotite-liquid equilibria and *P-T* estimates for biotite-bearing igneous rocks. *Contributions to Mineralogy and Petrology* **123**, 1–21.

Russell, J. K. & Nicholls, J. (1988). Analysis of petrologic hypotheses with Pearce element ratios. *Contributions to Mineralogy and Petrology* **99**, 25–35.

See, J. & Armstrong, T. (1988). Quantitative analysis of silicates and oxide minerals: comparison of Monte-Carlo, ZAF, and Phi-Rho-Z procedures. In: Newbury, D. E. (ed.) *Microbeam Analysis 1988: Proceedings of the 23rd Annual Conference of the Microbeam Analysis Society*. San Francisco: San Francisco Press, pp. 239–346.

Sharp, T. G., Otten, M. T. & Buseck, P. R. (1990). Serpentinization of phlogopite phenocrysts from a micaceous kimberlite. *Contributions to Mineralogy and Petrology* **104**, 530–539.

Skelton, A., Hode Vuorinen J., Arghe F. & Fallick, A. (2007). Fluid-rock interaction at a carbonatite-gneiss contact, Alno, Sweden. *Contributions to Mineralogy and Petrology* **154**, 75–90.

Smith, C. B., Sims, K., Chimuka, L., Duffin, A., Beard, A. D. & Townend, R. (2004). Kimberlite metasomatism at Murowa and Sese pipes, Zimbabwe. *Lithos* **76**, 219–232.

Stripp, G. R., Field, M., Schumacher, J. C., Sparks, R. S. J. & Cressey, G. (2006). Post-emplacement serpentinization and related hydrothermal metamorphism in a kimberlite from Venetia, South Africa. *Journal of Metamorphic Geology* **24**, 515–534.

Stubley, M. P. (2000). *Bedrock Geology of the Snap Lake Area, Camsell Lake Property*. A report to accompany a 1:10,000 scale geological map. Unpublished Report, Nelson, BC, Canada. Prepared for Winspear Resources Ltd, 35 pp.

Tracy, R. J. & Frost, B. R. (1991). Phase equilibria and thermobarometry of calcareous, ultramafic and mafic rocks and iron formations. In: Kerrick, D. M. & Ribbe, P. H. (eds) *Contact Metamorphism. Mineralogical Society of America, Reviews in Mineralogy and Geochemistry* **26**, 207–289.

White, J. L., Sparks R. S. J., Bailey, K., Barnett, W. P., Field, M. &Windsor, L. (2012). Kimberlite sills and dykes associated with the Wesselton kimberlite pipe. Kimberley, South Africa. *South African Journal of Geology* **115**, 1–32.